AWARD NUMBER:

W81XWH-13-1-0353

TITLE:

“Targeting the Adipocyte-Tumor Cell Interaction in Prostate Cancer Treatment”

PRINCIPAL INVESTIGATOR:

Maria T. Diaz-Meco, PhD

CONTRACTING ORGANIZATION:

Sandford-Burnham Medical Research Institute
La Jolla, CA 92037

REPORT DATE:

October 2014

TYPE OF REPORT:

Annual

PREPARED FOR: U.S. Army Medical Research and Materiel Command
Fort Detrick, Maryland 21702-5012

REPORT DOCUMENTATION PAGE

Form Approved
OMB No. 0704-0188

1. REPORT DATE	2. REPORT TYPE	3. DATES COVERED
October 2014	Annual	30 Sep 2013- 29 Sep 2014

4. TITLE AND SUBTITLE

"Targeting the Adipocyte-Tumor Cell Interaction in Prostate Cancer Treatment"

5a. CONTRACT NUMBER

5b. GRANT NUMBER
W81XWH-13-1-0353

5c. PROGRAM ELEMENT NUMBER

6. AUTHOR(S)

Maria T. Diaz-Meco, PhD

E-Mail: mdmeco@sbmri.org

5d. PROJECT NUMBER

5e. TASK NUMBER

5f. WORK UNIT NUMBER

7. PERFORMING ORGANIZATION NAME(S) AND ADDRESS(ES)

Sanford Burnham Medical Research Institute

La Jolla, CA 92037

8. PERFORMING ORGANIZATION REPORT NUMBER

9. SPONSORING / MONITORING AGENCY NAME(S) AND ADDRESS(ES)

U.S. Army Medical Research and Materiel Command
Fort Detrick, Maryland 21702-5012

10. SPONSOR/MONITOR'S ACRONYM(S)

11. SPONSOR/MONITOR'S REPORT NUMBER(S)

12. DISTRIBUTION / AVAILABILITY STATEMENT

Approved for Public Release; Distribution Unlimited

13. SUPPLEMENTARY NOTES

14. ABSTRACT

Prostate cancer (PCa) is one of the leading causes of death among men in the United States. Obesity is another growing epidemic health problem in Western societies and in developing nations, and represents one of the greatest threats to global human health. Several epidemiological studies during the last decade have pointed to an association between obesity and increased risk factor for PCa progression and aggressiveness. However, despite the relatively high amount of epidemiological data available, little is known about the molecular basis underlying the association between PCa progression, obesity and inflammation, and the role of the adipocyte-cancer cell interaction in this process. The goal of this project is to test the hypothesis that p62 is a molecular link in the cross-talk between obesity, inflammation and prostate cancer progression. Here, we have generated a new mouse model to address this question. Unveiling the molecular mechanisms governing obesity-induced prostate cancer progression will have a great impact in our understanding of this process, and its relevance for potential more targeted and efficacious therapies in PCa.

15. SUBJECT TERMS
Prostate cancer, obesity, inflammation, p62, metastasis, IL-6, adipocyte, mouse models, stroma, c-Myc, mTORC1

16. SECURITY CLASSIFICATION OF:			17. LIMITATION OF ABSTRACT	18. NUMBER OF PAGES	19a. NAME OF RESPONSIBLE PERSON
					USAMRMC
a. REPORT	b. ABSTRACT	c. THIS PAGE			19b. TELEPHONE NUMBER *(include area code)*
U Unclassified	U Unclassified	U Unclassified	UU Unclassified	46	

Table of Contents

Page

1. INTRODUCTION

Obesity substantially increases the risk of dying from prostate cancer (PCa), with higher body-mass index positively associated with more aggressive fatal disease [1,2]. Given the current obesity epidemic, it is urgent to explore possible interventions to disrupt the obesity-PCa link. Identifying the molecular mechanisms governing obesity-induced PCa progression will have a great impact on our understanding of this process, and will help in the design of more targeted and efficacious therapies in PCa. Collaborative efforts between our two laboratories (Diaz-Meco and Moscat) have identified p62 as a novel player in PCa and in obesity-induced inflammation, providing us with a unique in vivo model to study, at a cellular and molecular level, the mechanisms regulating the obesity-PCa interface. Understanding the role of p62 in the cellular and molecular pathways controlling PCa progression in obesity will generate high-impact information critical for the design of new therapeutic strategies aimed at targeting the tumor microenvironment. Interfering with adipocyte-tumor cell interactions to disrupt PCa progression could be a much-needed new therapeutic avenue.

2. KEYWORDS

Prostate cancer; obesity; inflammation; p62; tumor microenvironment; adipocyte; IL-6; mouse models; stroma; mTORC1; c-Myc

3. OVERALL PROJECT SUMMARY

This annual report corresponds to the first year of the Synergistic Idea Development Awards W81XWH-13-1-0353 (PI: Dr. Diaz-Meco) and W81XWH-13-1-0354 (Partnering PI: Dr. Moscat).

The goal of this synergistic project is to test the hypothesis that p62 is a molecular link that connects obesity, inflammation, and PCa progression. This will be addressed in three Specific Aims:

Aim 1. Investigate the in vivo role of p62 in the relationship between adipose tissue and PCa progression.

Aim 2. Determine the role of p62-mediated inflammation in the PCa tumor microenvironment.

Aim 3: Explore the role of p62 in the adipocyte-PCa cell interaction through cellular and mechanistic in vitro studies.

The overall progress of the project has been highly satisfactory and we have completed successfully an important part of the proposed study. According to the approved SOW we have performed the following tasks corresponding to this period:

Task 1: Breeding of the required mice for experiments (Months 1-16; Diaz-Meco & Moscat)

Task 1.1. Diaz-Meco lab has started the breeding of TRAMP+ mice with $p62^{Adipo}$ mice provided by Moscat lab. Final crosses with the adequate genotype have been set up for the generation of the required experimental mice. No major problems have been encountered with the breeding of these mice. Breeding will be continued to generate enough mice of the correct genotype for Tasks 2-5 and necessary for Aim 1.

Task 1.2. Moscat lab has already bred WT, p62 KO, IL-6 KO and p62/IL-6 DKO mice to be used in Task 6 as part of Aim 2.

Task 2: Analysis of the PCa phenotype of $TRAMP^{+}/p62^{Adipo}$ and $TRAMP^{+}$ mice (Months 4-16; Diaz-Meco)

Task 2.1. Disease-free survival curves (Kaplan-Meier plots) are underway and will be completed in the next year period of the project.

Task 2.2. Analysis of PCa progression in TRAMP^{+}/p62^{Adipo} and TRAMP^{+} mice: Diaz-Meco lab has started the characterization of the phenotype of TRAMP^{+}/p62^{Adipo}. Although not enough mice of the correct genotype and adequate age are yet available to complete our analysis, our preliminary data are very promising. Interestingly, we have found that TRAMP^{+}/p62^{Adipo} mice developed a more aggressive phenotype with higher incidence of metastasis in liver, lung and kidney as compared to TRAMP^{+} mice controls (Fig. 1). Four littermates TRAMP and TRAMP^{+}/p62^{Adipo} mice of 36 wks of age were analyzed. Genotype was confirmed by PCR and by western-blot for p62 in the different tissues. p62 was selectively deleted in WAT of TRAMP^{+}/p62^{Adipo} and not in other tissues such as prostate or liver (Fig. 1A). Consistent with our preliminary data of p62^{Adipo} mice, TRAMP^{+}/p62^{Adipo} mice also displayed a higher body weight than age-matched TRAMP^{+} littermate controls (Fig. 1B). Of note, we found metastasis in liver, lung and kidney in TRAMP^{+}/p62^{Adipo} mice whereas no metastasis was detected in TRAMP^{+} littermate controls (Fig. 1C-D). Characterization by immunostaining of liver metastasis confirmed their neuroendocrine origin with a positive staining for synaptophysin and negative for androgen receptor (Fig. 1E). These results suggest that the loss of p62 selectively in the adipose tissue drives tumorigenesis and invasiveness in PCa. This is consistent with the epidemiological data indicating that obesity increases the risk of dying from PCa[1,2] and offers a molecular link to start dissecting the mechanism connecting adipocytes and PCa progression.

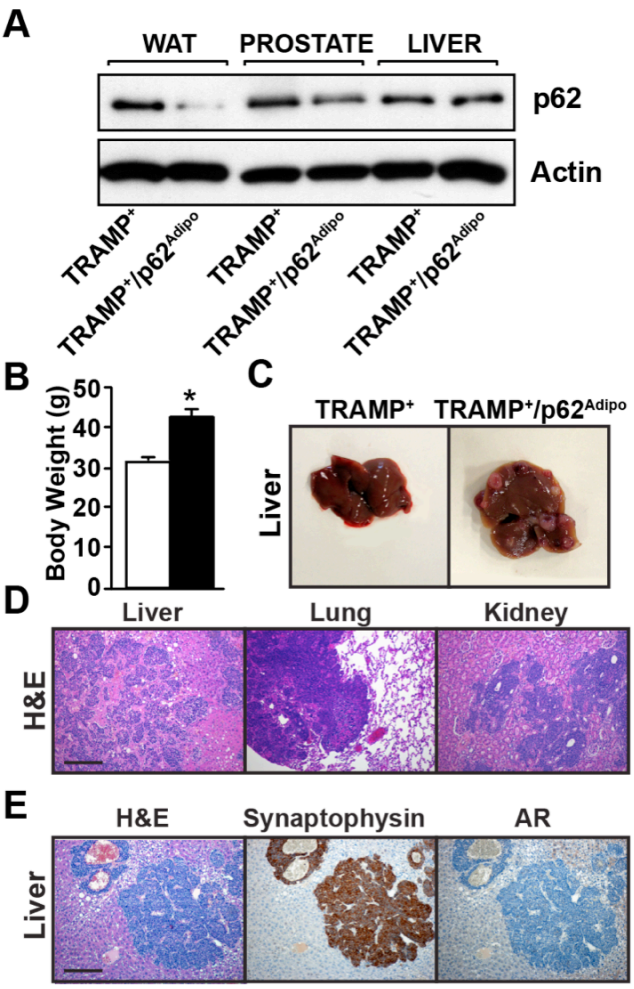

Figure 1. p62-deficiency in the adipose tissue promotes metastasis (A) Immunoblots for p62 and actin of total protein extracts from BAT, prostate and liver from TRAMP^{+} and TRAMP^{+}/p62^{Adipo} mice. **(B)** Graph showing body weight of TRAMP^{+} and TRAMP^{+}/p62^{Adipo} mice. **(C)** Representative pictures of liver from TRAMP^{+} and TRAMP^{+}/p62^{Adipo} mice at 36 weeks of age. **(D)** Representative pictures of H&E staining of liver, lung and kidney metastases from TRAMP^{+}/p62^{Adipo} mice. **(E)** H&E and immunostaining of synaptophysin and androgen

Task 3: Analysis of the general metabolic characterization of TRAMP+/p62Adipo and TRAMP+ mice (Months 4-16; Moscat). A cohort of 6 mice of each genotype has been generated and genotype has been confirmed. These mice will be analyzed for metabolic studies (CLAMS and DXA) in February 2014, when they reach the adequate age for analysis. Based on our preliminary data in Task 2, we will perform metabolic analysis at 9 month of age instead of 10 months of age, as initially planned due to limited survival of the TRAMP+/p62Adipo mice.

Task 6. In vivo characterization of inflammation in PCa tumors, and adipose tissue (Months 23-30; Diaz-Meco & Moscat).

Although this task was planned to be performed during the 3rd year of the project, we decided to start tackling this part of the study while we wait for more TRAMP+/p62Adipo mice to be available for analysis. Since Moscat lab generated in Task 1.2 enough WT, p62 KO and p62/IL-6 DKO mice, we decided to perform the experiments described in Tasks 6.2-6.7 to address the role of p62-mediated

inflammation in the PCa tumor microenvironment (Aim 2). Tasks 6.2 to 6.6 have been completed and we have set up all the conditions and generated preliminary data for Task 6.7.

Tasks 6.2-6.6 (Aim 2.2). Determine the role of IL-6 in PCa in vivo. (Diaz-Meco & Moscat). These tasks have been completed. Here we have tested the hypothesis that p62-deficiency-induced obesity promotes carcinogenesis through increased adipose tissue and systemic inflammation, resulting in enhanced IL-6 production. To address the in vivo role of IL-6 in the p62-deficient tumor microenvironment, we have performed orthotopic injections of PCa cells into the prostates of WT, p62

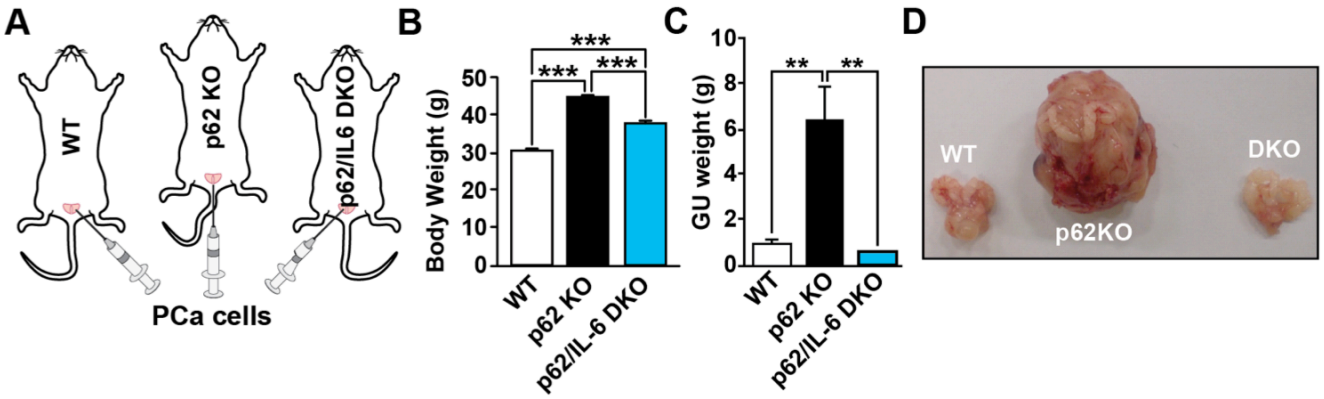

Figure 1. IL-6 is required for p62's role in the tumor microenvironment. (A) Orthotopic injection of TRAMP-C2Re3 cells into the prostates of syngeneic WT and p62 KO mice. Orthotopic tumors were allowed to grow for two months. **(B)** Body weight. **(C)** GU tract weight. **(D)** Pictures of representative orthotopic tumors . n = 5 or 6 mice per genotype.

KO and p62/IL-6 DKO mice (Fig 2A) and body weight (Fig. 2B) and genitourinary weight (Fig. 2C) was determined. Consistent with our preliminary data presented in the Project Narrative, orthotopic tumors grew faster in the prostates of p62 KO mice as compared with WT controls, and importantly, tumor growth was completely abolished when the injections were performed in the p62/IL6 DKO prostates, indicating that IL-6 is required in vivo for the role of p62 in the tumor microenvironment (Fig. 2D). Due to limitation in material since the p62/IL6 DKO tumors were very small, the staining was only performed in WT and p62 KO tumors and the DKO tumors were reserved for RNA analysis. H&E staining of the orthotopic tumors grown in p62 KO mice showed infiltration of periprostatic adipocytes into the tumor whereas in the WT tumors the adipocytes were restricted to the periphery (Fig 3). In addition, p62 KO tumors have a higher proliferation rate as measured by Ki67 staining (Fig. 4A and 4C). No changes were observed in apoptosis as detected by staining with cleaved Caspase-3 (Fig. 4B and 4D).

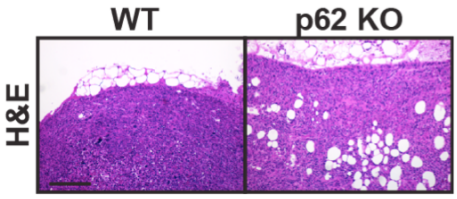

Figure 3. **Infiltration of adipocytes in orthotopic tumors of p62 KO.** H&E staining of orthotopic tumors from WT and p62 KO mice. Scale bar = 200 mm.

To address which is the cellular compartment responsible for p62 actions in the tumor microenvironment, we used an in vitro 3D organotypic system. This 3D model allows us to recapitulate in an in vitro amenable system the tumor microenvironment and its interactions with the tumor cell, closely mimicking the physiological situation [3]. Using this system, we initially tested whether fibroblasts and/or macrophages play a role in mediating p62 function in the tumor microenvironment. To do that, we combined PCa cells with fibroblasts, or macrophages obtained from mice of the different genotypes. After cultures, gel were fixed and processed for H&E staining and invasion was quantified. Of note, fibroblasts were able to recapitulate the p62 KO phenotype in the tumor microenvironment, whereas macrophages had no effect. Importantly, this effect was also

completely reverted in p62/IL6 DKO (**See Appendix, Fig. 3 and S3**). This reinforces the notion that IL6 is critical to mediate p62 actions in the prostate tumor micro-environment. However, since p62 KO mice are obese and display higher fat content and orthotopic tumors from p62 KO had infiltrated adipocytes (Fig. 3), we will also test the potential role of adipocytes in this system. This will be address in Task 7 in next period.

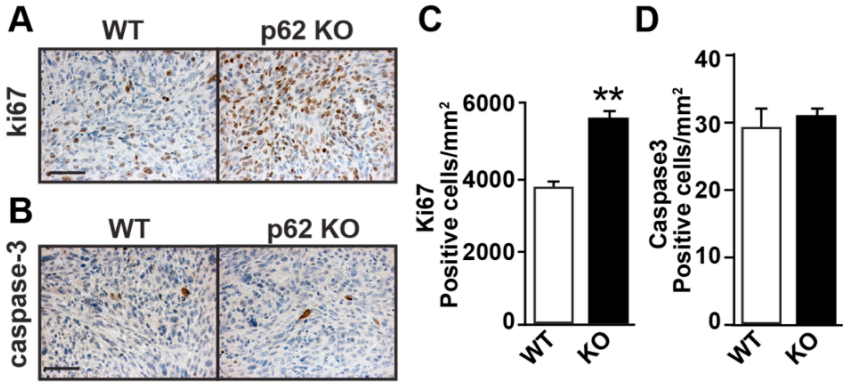

Figure 4. Increased proliferation in p62 KO orthotopic tumors. (A-B) Immunostaining of Ki67 (A) and cleaved caspase 3 **(B)** in orthotopic tumors of WT and p62 KO mice. **(C-D)** Quantification of Ki67-positive cells **(C)** and caspase3 positive cells **(D)**. Results are the means ± SEM of counts from

Notably, the results from these Tasks have been recently published in the top-notch journal **Cancer Cell** [4](see Appendix) as part of a study on the novel role of p62 as a tumor suppressor in the tumor microenvironment in PCa. In this study, we showed that p62 levels were downregulated in stromal cells of primary human prostate tumors, and that decreased p62 expression was correlated with progression to aggressive tumors. The loss of p62 allowed for enhanced tumor growth and induced an activated, cancer-associated fibroblast–like phenotype in the tumor stroma, characterized by upregulation of TGFβ and IL6. This inflammatory phenotype in p62-deficient stroma promoted a metabolic deregulation mediated by inhibition of mTOR complex 1 (mTORC1) and subsequent repression of c-Myc. These results demonstrate a critical role for stromal p62 as a tumor suppressor and support targeted inhibition of the tumor microenvironment as a therapeutic approach to limit tumor progression. Importantly, we also showed that mTORC1 and c-Myc, like p62, although they are oncogenes upregulated in PCa epithelial cells, they behave as a tumor suppressor in the stroma. This has important implications from a therapeutic point of view because inhibition of p62 and/or mTORC1 may result in opposite effects in the stroma and the epithelium of the tumor, thus reducing the efficacy of broadly applied mTORC1-based chemotherapeutic approaches.

Tasks 6.7. (Aim 2.3) Determine the role of adipose-stem cells (ASC). Since fibroblasts and adipocytes have the same cell of origin [5], it would be of great interest to further investigate whether p62 regulates mesenchymal stem cells in PCa. To start addressing this question, we have first determined the adipose stem cell population in adipose tissue of TRAMP+/p62Adipo and TRAMP+ mice and of WT and p62 KO. A schematic description of the method of isolation of ASCs is described in Fig. 5A. Briefly, adipose tissue was excised and the SVF isolated as described [6]. The isolated SVF was resuspended in ice-cold Dulbecco's modified Eagle's medium (DMEM) with 2% fetal bovine serum (FBS) for labeling. Antibody incubations were performed on ice for 20 min. Cells were washed and resuspended in Hank's balanced salt solution (HBSS) with DAPI for sorting. For sorting, cells were initially selected by size, on the basis of forward scatter (FSC) and side scatter (SSC), followed by exclusion of dead cells on the basis of uptake of DAPI. Then, live cells were gated on both SSC and FSC singlets, ensuring that the staining of individual cells was analyzed. Next, the cells were separated on the basis of the cell-surface markers indicated. p62 deficiency in ASCs was confirmed by qRT-PCR of p62 levels in ASCs isolated from mice of the different genotypes (Fig. 5B). Of note, we found that adipose tissue from both TRAMP+/p62Adipo or p62 KO had more ASCs than their corresponding controls

(Fig. 5C-D). This is a very interesting result that suggests that there is in fact an expansion of the ASC population as a consequence of p62-deficiency. Therefore, we will next investigate during the next period whether these ASCs are more infiltrated in the orthotopic tumors.

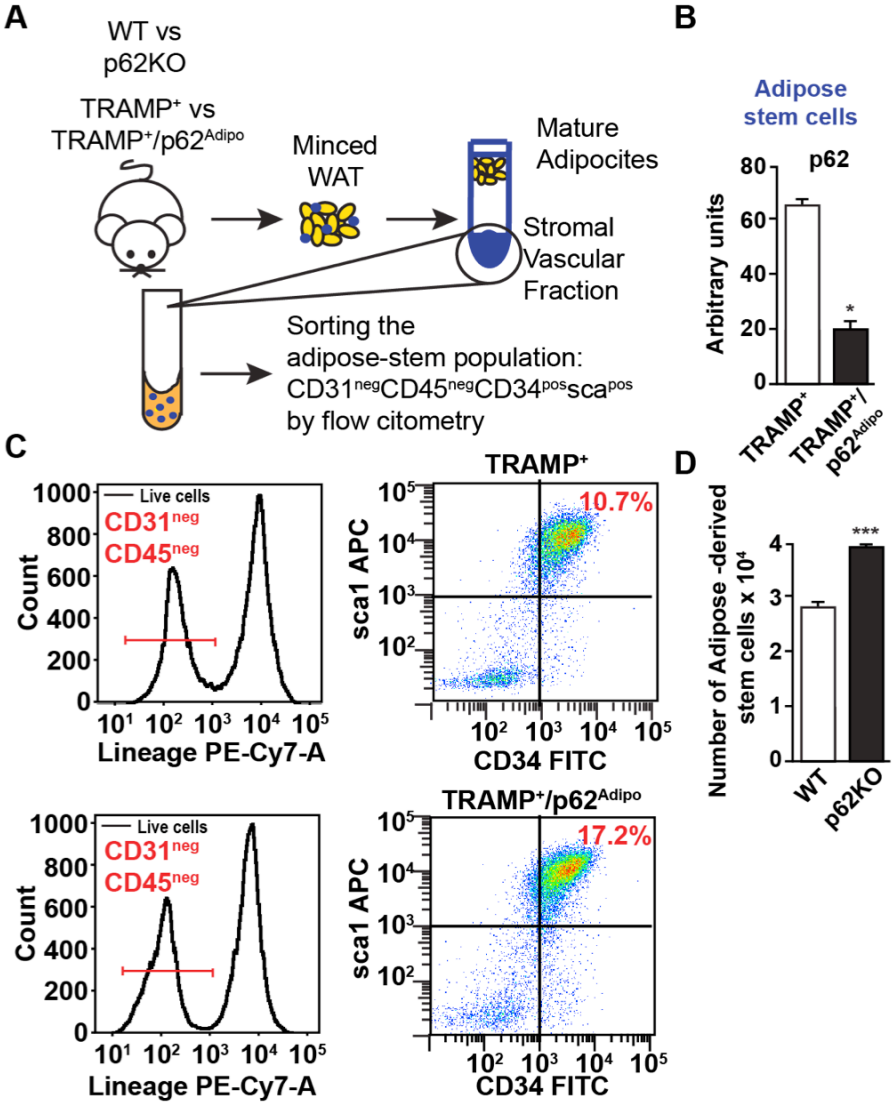

Figure 5. (A) Schematic representation of FACS-purification of adipose-derived stem cells from white adipose tissue of the indicated genotypes. **(B)** RT-PCR of p62 from adipose-derived stem cells of TRAMP^{+} and TRAMP^{+}/p62^{Adipo} mice. **(C)** Histograms and dot-plots showing FACS staining profiles and gating of adipose stem cells from TRAMP^{+} and TRAMP^{+}/p62^{Adipo} mice. The live cells were sorted for CD31^{neg}CD45^{neg} (histograms in the left). These cells were then sorted on the basis of expression of CD34 and sca1 (dot plots in the right). The percentage yield of CD31^{neg}CD45^{neg}CD34^{pos}sca1^{pos} cells (adipose-derived stem cells) for each genotype is indicated. **(D)** Quantification of adipose-derived stem cells from WT and p62KO mice isolated as described above. *p<0.05, ***p<0.001.

4. KEY RESEARCH ACCOMPLISHMENTS

- Identification of p62 as a novel tumor suppressor in the stroma in PCa.
- Demonstration that p62-mediated inflammation in the stroma is key for prostate tumorigenesis.
- Identification of the inflammatory cytokine IL-6 as a major player in mediating p62 actions in the tumor stroma.
- Characterization of a molecular network linking p62 to mTORC1 and c-Myc operating in the stroma to influence tumorigenesis in the prostate epithelium.
- Identification of c-Myc as a novel tumor suppressor in the stroma in PCa, opposite to its role as an oncogene in the epithelium.
- The use of mTORC1 inhibitors in PCa could have deleterious effect through its role in the stroma.
- The identification of the mechanisms that reduce p62 levels in the stroma could constitute a novel strategy to intervene in PCa.
- p62 deficiency in the adipose tissue expands the adipose-stem cell population.
- p62 selective deficiency in the adipose tissue promotes a more aggressive PCa phenotype, providing a link between obesity and adiposity and PCa progression.

5. CONCLUSION

The results generated during this year have allowed us to demonstrate that p62 is a novel tumor suppressor in the prostate tumor stroma. We have unveiled its mechanism of action through metabolic reprograming that is initiated by an inflammatory response. We have identified IL-6 as a key inflammatory mediator for p62 actions in the stroma. Furthermore, we have initiated the generation of a new mouse model to study the link of obesity and PCa by selective deletion of p62 in the adipose tissue and in the context of the TRAMP model. Our preliminary data are very promising and suggest that p62 deficiency in the adipose tissue promotes a more aggressive phenotype. In the next period we will study the metabolic mechanism, at whole body level as well as a cellular level, that underlies this phenotype. Our goal is to identify potential new targets to disrupt the obesity-PCa link.

6. PUBLICATIONS, ABSTRACTS, AND PRESENTATIONS

Publications:

✓ Peer-Reviewed Scientific Journals:

Valencia, T., Kim, J.Y., Abu-Baker, S., Moscat-Pardos, J., Ahn, C.S., Reina-Campos, M., Duran, A., Castilla, E.A., Metallo, C.M., Diaz-Meco, M.T.*, and Moscat, J*. (2014) Metabolic reprogramming of stromal fibroblasts through p62-mTORC1 signaling promotes inflammation and tumorigenesis. **Cancer Cell** 26, 121-135 (*equal contribution and corresponding author)

This publication has been highlighted in the following scientific articles:

- Ubaldo E. Martinez-Outschoorn, Federica Sotgia, Michael P. Lisanti. (2014). Metabolic Asymmetry in Cancer: A "Balancing Act" that Promotes Tumor Growth. **Cancer Cell**, Volume 26, Issue 1, 14 July 2014, 5-7
- Research Watch: Tumor Microenvironment: p62 loss reprograms stromal metabolism to promote tumor growth. (2014) **Cancer Discovery** Published Online First July 17, 2014; doi:10.1158/2159-8290.CD-RW2014-152
- Alderton, G.K. (2014). Stromal metabolism has paracrine effects. Nature Reviews **Cancer**, Research Highlight. 14, 515.

✓ Lay press:

Our publication in Cancer Cell has been reviewed in several lay articles:

Newswise – La Jolla, CA, July 3, 2014. "New study reveals how tumors remodel their surroundings to grow"

EurekAlert. AAAS, July 3, 2014. "New study reveals how tumors remodel their surroundings to grow"

Science Daily. July 3, 2014. "How tumors remodel their surroundings to grow".

Abstracts and presentations:

"Nutrient sensing and Cancer Metabolism by the p62 autophagy pathway" University of Pennsylvania, Philadelphia, 2014. Speaker (Moscat).

"New role of metabolic reprograming in stroma-induced tumorigenesis" Centre for Genome Regulation, Barcelona, Spain, 2014. Speaker (Moscat).

"Metabolic Reprogramming by the p62 Pathway in Cancer" in the "2014 ASIP Annual Meeting at Experimental Biology 2014" (San Diego, 2014). Speaker (Moscat).

"mTORC1 activation by p62" in the SBMRI Workshop on "Cancer Metabolism, autophagy and nutrient sensing" (La Jolla, USA, 2014). Speaker and co-organizer (Moscat)

"Metabolic reprograming by the mTORC1/p62 complex in the tumor stroma" in the SBMRI Workshop on "Cancer Metabolism, autophagy and nutrient sensing" (La Jolla, USA, 2014). Speaker and co-organizer (Diaz-Meco)

"Metabolic reprogramming in the stroma promotes inflammation and tumorigenesis". CDSN / MDP Metabolism Retreat. (Carlsbad, USA, 2014). Speaker (Diaz-Meco)

7. INVENTIONS, PATENTS AND LICENSES

Nothing to report.

8. REPORTABLE OUTCOMES

- New mouse model to study the link of obesity and prostate cancer.
- New 3D organotypic model to provide a physiological and amenable system to study the biology and the relationships of the different cell types in the tumor microenvironment.

- A manuscript in Cancer Cell co-authored by both laboratories (Moscat and Diaz-Meco) as an example of the synergy created with this award (see above in Publications)

9. OTHER ACHIEVEMENTS

Nothing to report.

10. REFERENCES

1. Haque, R.*, et al.* Association of body mass index and prostate cancer mortality. *Obesity research & clinical practice* **8**, e374-381 (2014).
2. Joshu, C.E.*, et al.* Weight gain is associated with an increased risk of prostate cancer recurrence after prostatectomy in the PSA era. *Cancer Prev Res (Phila)* **4**, 544-551 (2011).
3. Ridky, T.W., Chow, J.M., Wong, D.J. & Khavari, P.A. Invasive three-dimensional organotypic neoplasia from multiple normal human epithelia. *Nat Med* **16**, 1450-1455 (2010).
4. Valencia, T.*, et al.* Metabolic Reprogramming of Stromal Fibroblasts through p62-mTORC1 Signaling Promotes Inflammation and Tumorigenesis. *Cancer Cell* **26**, 121-135 (2014).
5. Uccelli, A., Moretta, L. & Pistoia, V. Mesenchymal stem cells in health and disease. *Nat Rev Immunol* **8**, 726-736 (2008).
6. Rodbell, M. Metabolism of Isolated Fat Cells. I. Effects of Hormones on Glucose Metabolism and Lipolysis. *J Biol Chem* **239**, 375-380 (1964).

11. APPENDICES

Publication:

Valencia, T., Kim, J.Y., Abu-Baker, S., Moscat-Pardos, J., Ahn, C.S., Reina-Campos, M., Duran, A., Castilla, E.A., Metallo, C.M., Diaz-Meco, M.T.*, and Moscat, J*. (2014) Metabolic reprogramming of stromal fibroblasts through p62-mTORC1 signaling promotes inflammation and tumorigenesis. **Cancer Cell** 26, 121-135 (*equal contribution and corresponding author)

Cancer Cell
Article

Metabolic Reprogramming of Stromal Fibroblasts through p62-mTORC1 Signaling Promotes Inflammation and Tumorigenesis

Tania Valencia,[1] Ji Young Kim,[1] Shadi Abu-Baker,[2] Jorge Moscat-Pardos,[1] Christopher S. Ahn,[3] Miguel Reina-Campos,[1] Angeles Duran,[1] Elias A. Castilla,[2] Christian M. Metallo,[3,4] Maria T. Diaz-Meco,[1,5,*] and Jorge Moscat[1,5,*]
[1]Sanford-Burnham Medical Research Institute, 10901 N. Torrey Pines Road, La Jolla, CA 92037, USA
[2]University of Cincinnati Medical College, Cincinnati, OH 45267, USA
[3]Department of Bioengineering, University of California, San Diego, 9500 Gilman Drive, La Jolla, CA 92093, USA
[4]Moores Cancer Center, University of California, San Diego, 9500 Gilman, Drive, La Jolla, CA 92093
[5]Co-senior author
*Correspondence: mdmeco@sanfordburnham.org (M.T.D.-M.), jmoscat@sanfordburnham.org (J.M.)
http://dx.doi.org/10.1016/j.ccr.2014.05.004

SUMMARY

The tumor microenvironment plays a critical role in cancer progression, but the precise mechanisms by which stromal cells influence the epithelium are poorly understood. Here we show that p62 levels were reduced in the stroma of several tumors and that its loss in the tumor microenvironment or stromal fibroblasts resulted in increased tumorigenesis of epithelial prostate cancer cells. The mechanism involves the regulation of cellular redox through an mTORC1/c-Myc pathway of stromal glucose and amino acid metabolism, resulting in increased stromal IL-6 production, which is required for tumor promotion in the epithelial compartment. Thus, p62 is an anti-inflammatory tumor suppressor that acts through the modulation of metabolism in the tumor stroma.

INTRODUCTION

Primary tumors are initiated as a result of the stepwise acquisition of genetic alterations within the epithelial compartment (Shen and Abate-Shen, 2010). However, increasing evidence supports the notion that the tumor microenvironment also plays a critical role in cancer progression in many types of neoplasias, including prostate cancer (PCa), although relatively little is known about the signaling pathways that mediate communication between the stromal and epithelial compartments (Ammirante et al., 2010; Erez et al., 2010; Santos et al., 2009; Trimboli et al., 2009). Inflammation and metabolism are two critical factors contributing to the protumorigenic properties of the stroma (DeBerardinis and Thompson, 2012; Grivennikov et al., 2010; Hanahan and Coussens, 2012; Metallo and Vander Heiden, 2013; Vander Heiden, 2013). Although not totally understood, some evidence suggests that the metabolic state of the tumor stroma can decisively influence the tumorigenic potential of the tumor epithelial compartment (Lisanti et al., 2013). Here we have addressed this fundamental biological question in the context of p62 deficiency in the nonepithelial tumor compartment. Our laboratory initially identified p62, also known as sequestosome-1, as a scaffold protein for the atypical protein kinase C isozymes and later implicated p62 in other cell stress responses (Diaz-Meco and Moscat, 2012; Moscat and Diaz-Meco, 2012; Moscat et al., 2007; Sanchez et al., 1998). p62 binds Raptor, a key component of the mTOR-orchestrated nutrient-sensing complex and an important activator of anabolic pathways that are instrumental in metabolic reprogramming during cell transformation (Duran et al., 2011; Moscat and Diaz-Meco, 2011). Nonetheless, nothing is known about the signaling cascades that p62 regulates in stromal cells or to

Significance

Inappropriate activation of the stroma as a consequence of the tumorigenic process can potentiate the growth and transformation of epithelial tumor cells, thus facilitating the progression of cancers toward more malignant stages. Using prostate cancer as a model system, we show that the loss of the signaling adaptor p62 in stromal cells triggers an inflammatory response that leads to activation of cancer-associated fibroblasts that enhances tumorigenesis in vitro and in vivo. Deficiency in p62 results in reduced mTORC1 activity and deregulation of metabolic pathways controlling inflammation. Because the stroma is increasingly recognized as a potential source of therapeutic targets, this study suggests that targeting stromal metabolic reprogramming can decisively influence the tumorigenic potential of the tumor epithelial compartment.

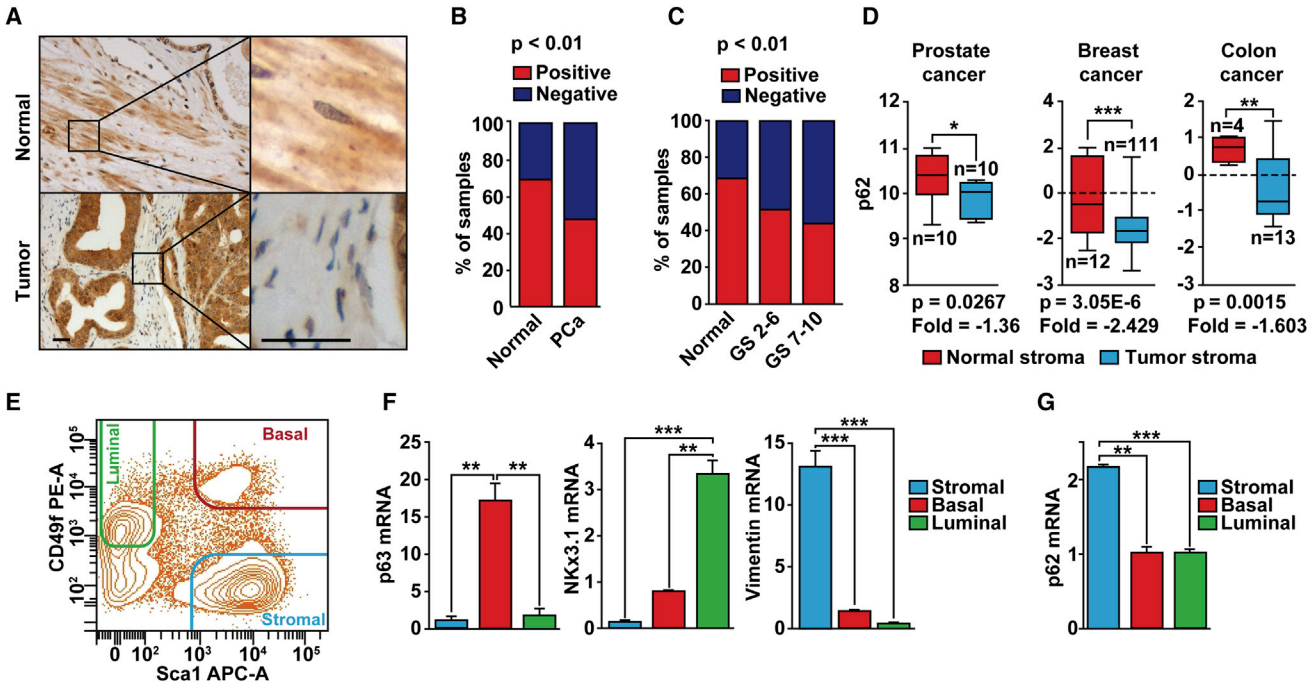

Figure 1. p62 Levels Are Reduced in the Stroma of Human Prostate Tumors

(A) Representative examples of p62 staining of normal and primary prostate cancer (tumor) samples. The scale bars represent 25 μm.

(B) Quantification of p62 staining in the stroma of primary PCa tumors compared with normal; n = 22 (normal), n = 202 (PCa). Fisher's exact test, $p < 0.01$.

(C) p62 levels are reduced upon PCa progression; n = 22 (normal), n = 70 (GS 2–6), n = 132 (GS 7–10). Chi-square test, $p < 0.01$.

(D) p62 mRNA levels in stroma of human cancer samples. Data were collected from public data sets of gene expression in the tumor stroma of several human cancers: GSE34312 (prostate cancer), GSE9014 (breast cancer), and GSE35602 (colon cancer).

(E) FACS-sorted adult murine prostate cell lineages. Prostate basal, luminal, and stromal cells are $Lin^{-}Sca\text{-}1^{+}CD49f^{Hi}$, $Lin^{-}Sca\text{-}1^{-}CD49f^{Low}$, and $Lin^{-}Sca\text{-}1^{+}CD49f^{-}$, respectively.

(F) RT-PCR of specific markers for each prostate cell population (n = 3): p63 (basal), Nkx3.1 (luminal), and vimentin (stromal).

(G) RT-PCR for p62 in prostate cell populations (n = 3).

*$p < 0.05$, **$p < 0.01$, ***$p < 0.001$. Results are presented as mean ± SEM. See also Figure S1.

what extent these pathways influence the epithelial-stromal interaction in the tumor microenvironment. Cancer-associated fibroblasts (CAFs) have been proposed to be key mediators of the crosstalk between malignant tumor cells and their microenvironment (Barron and Rowley, 2012; Franco and Hayward, 2012). CAFs and the complex set of signaling molecules they secrete generate an environment conducive to inflammation, and this in turn maintains the protumorigenic status of the stromal cells. Among these proteins, interleukin-1β (IL-1β), interleukin-8, and interleukin-6 (IL-6) have been implicated as part of the proinflammatory signature of the PCa stroma (Erez et al., 2010; Franco and Hayward, 2012; Schauer et al., 2008). Furthermore, IL-6 has received increasing attention as a key proinflammatory and protumorigenic molecule in many types of cancer, including PCa (Azevedo et al., 2011; De Marzo et al., 2007; Guo et al., 2012; Schafer and Brugge, 2007). Here we address the role of p62 in the stroma in the control of the inflammatory environment in PCa.

RESULTS

p62 Expression Levels in the Tumor Microenvironment

The initial evidence suggesting that p62 plays a role in the regulation of the tumor microenvironment in PCa came from the histological analysis of a tissue panel comprising 202 primary human PCa tumors, 8 metastases, and 22 adjacent normal prostate tissue samples. This study revealed that p62 was expressed in the prostate epithelium and also in the stroma (Figure 1A). p62 protein levels were downregulated in the stroma of human primary PCa tumors compared with the stroma of normal samples (Figures 1A and 1B). Furthermore, when the tumor samples were grouped on the basis of low Gleason score (GS) (2–6) or high GS (7–10), p62 levels in the stroma were significantly reduced upon progression to the most aggressive stage (Figure 1C). p62 was also overexpressed in the epithelial compartment of the PCa human samples (Figure 1A; Figures S1A and S1B available online). This is consistent with previous observations suggesting that p62 is upregulated in many cancers, including lung cancer (Duran et al., 2008; Inoue et al., 2012), liver cancer (Inami et al., 2011), glioblastoma (Galavotti et al., 2013), breast cancer (Rolland et al., 2007; Thompson et al., 2003), and kidney cancer (Li et al., 2013). However, because those studies did not report on expression in the stromal component, it is not clear whether p62 was downregulated in the stroma in those samples, as we have shown in the samples analyzed here. Moreover, bioinformatics analysis of public data sets of stromal gene expression also demonstrated that p62 was significantly downregulated in the tumor stroma, compared

with normal stroma, in several types of cancers, including prostate, breast, and colon cancers (Figure 1D). In addition, fluorescence-activated cell sorting (FACS) analysis of adult mouse prostates showed that p62 is more highly expressed in cells of the stroma than in those of basal or luminal lineages (Figures 1E–1G). Quantitative RT-PCR analyses of the sorted prostate cell populations showed that transcripts for the basal marker p63, the luminal cell marker Nkx3.1, and the stroma marker vimentin were enriched in their corresponding cell populations, demonstrating successful cell fractionation (Figures 1E and 1F). Of note, p62 expression was highly enriched in the stromal compartment compared with the other two cell populations (Figure 1G). These results suggest that p62 could exert its effect as a tumor suppressor in the tumor microenvironment, likely in the stroma.

p62 Is a Suppressor of Inflammation and the CAF Phenotype in the Tumor Microenvironment

To test whether p62 deficiency in the tumor microenvironment is relevant to the transforming properties of epithelial cells, we performed orthotopic injections of syngeneic murine PCa cells (TRAMP-C2Re3) (Olson et al., 2006) into the prostates of wild-type (WT) and p62 knockout (KO) mice and then assessed tumor growth. The resulting tumors were bigger in the prostates of p62 KO mice than in those of WT mice (Figures 2A–2C), supporting the notion that a loss of p62 in the tumor microenvironment promotes PCa growth. We next carried out transcriptomic profiling of the orthotopic tumors in the WT and p62 KO mice. NextBio analysis revealed important correlations between genes upregulated in the p62 KO orthotopic tumors with a gene signature in the category of "response to wounding" (Figure S2A). In addition, gene set enrichment analysis (GSEA) also identified "response to wounding" as significantly enriched of the gene ontology (GO) biological-process categories (Figure 2D; Figures S2B and S2C) and "stromal stimulation" in the C2 curated gene set library (Figures S2D and S2E). Because CAFs acquire an "activated phenotype" during tumor progression that resembles that of fibroblasts during the wound-healing repair process, these results suggested that the p62 KO stroma is likewise activated (Barron and Rowley, 2012; Bissell and Radisky, 2001; Franco and Hayward, 2012; Schäfer and Werner, 2008) and has a more CAF-like phenotype than the WT stroma. In support of this notion, we observed an increase in the expression of α smooth muscle actin (α-SMA) in sections from orthotopic tumors in p62 KO mice compared to WT controls (Figure 2E), as well as an increase in transforming growth factor β (TGF-β) transcripts as determined by RT-PCR in the same samples (Figure 2F). TGF-β and α-SMA are two bona fide markers of the CAF phenotype (Barron and Rowley, 2012; Franco and Hayward, 2012). Consistent with this, Ingenuity Pathway Analysis identified TGF-β1 as a predicted upstream regulator in the p62 KO orthotopic tumors ($p = 1.47 \times 10^{-7}$, activation Z score = 3.890). To determine the potential cell-autonomous effect of p62 in this important function, we used FACS to isolate prostate stromal cells from mice of both genotypes, as described in Figures 1E and 1F. Interestingly, we found that p62-deficient stromal cells also showed characteristics of CAFs, as determined by increased expression levels of α-SMA, TGF-β, and vimentin (Figure 2G). To facilitate subsequent studies, we generated prostate fibroblasts from WT and p62 KO mice and determined their "CAF activation" state. In these cells, the loss of p62 resulted in increased CAF transcript markers (Figure 2H), as well as in the secretion of TGF-β, as determined by ELISA (Figure 2I). This is important because TGF-β is essential for the acquisition and maintenance of the CAF/myofibroblast phenotype (Kojima et al., 2010; Ostman and Augsten, 2009). Therefore, p62 loss modifies the stroma by inducing a CAF phenotype, which in turn drives tumor progression.

Further bioinformatics GSEA revealed a hyperinflammatory phenotype in the p62 KO orthotopic tumors. That is, we found "humoral immune response" and "inflammatory response" as second GO categories enriched in the p62 KO transcriptome profile (Figure 2J; Figures S2F and S2G). RT-PCR analysis of the tumors from p62 KO mice showed increases in the transcripts of inflammatory cytokines such as IL-6, IL-1β, and keratinocyte chemoattractant (Figure 2K), as well as in the secretion of IL-6 as determined by ELISA (Figure 2L). We hypothesized that IL-6 could be an important mediator of the stromal p62-dependent signals that influence PCa progression in the epithelium. To test this possibility, we carried out an orthotopic injection experiment using p62/IL-6 double-KO (DKO) mice as hosts. Notably, the increased tumor growth observed in p62 KO mice was completely reversed in the DKO mice (Figures 2M and 2N), demonstrating that p62 plays a tumor-suppressive role in the tumor microenvironment during PCa progression by inhibiting CAF activation and blocking inflammation.

p62 in Stromal Fibroblasts Regulates an IL-6/TGF-β Cascade Essential for Tumor Invasion

We next set up a 3D organotypic culture model that recapitulates, in a genetically accessible system, the tumor microenvironment and its interactions with the tumor epithelial cell, closely mimicking the physiological situation and the cellular architecture (Gaggioli et al., 2007; Kim et al., 2013; Nyström et al., 2005; Ridky et al., 2010). Because our genome-wide transcriptomic analysis suggested that the loss of p62 in the tumor microenvironment is associated with a CAF-like signature, and because fibroblasts are a critical component of the stroma, we next tested whether p62 KO prostate fibroblasts were able to recapitulate the in vivo phenotype in 3D organotypic cultures. To do this, we cocultured in this organotypic system prostate fibroblasts from p62 KO and WT mice with TRAMP-C2Re3 PCa cells (Figure 3A). Importantly, p62 KO prostate fibroblasts (versus WT counterparts) enhanced the invasiveness and proliferation index of PCa epithelial tumor cells (Figures 3B–3D). Similar results were obtained with other PCa cell lines, such as mouse Myc-CaP (Figure S3A), or human PC3 cells (Figure S3B). Mouse fibroblasts from p62 KO mice also enhanced the invasiveness and proliferation index of human normal prostate epithelial cells compared with similar organotypic cultures with WT fibroblasts (Figure S3C). Altogether, this indicates that p62 deficiency in the stromal fibroblasts has a pivotal role in mediating cancer cell proliferation and invasion.

To follow up on our findings that IL-6 levels were increased in orthotopically injected tissues and that increased IL-6 expression was associated with enhanced tumorigenicity in vivo (Figures 2K–2N), we further investigated the role of this cytokine in the protumorigenic microenvironment created by p62 deficiency

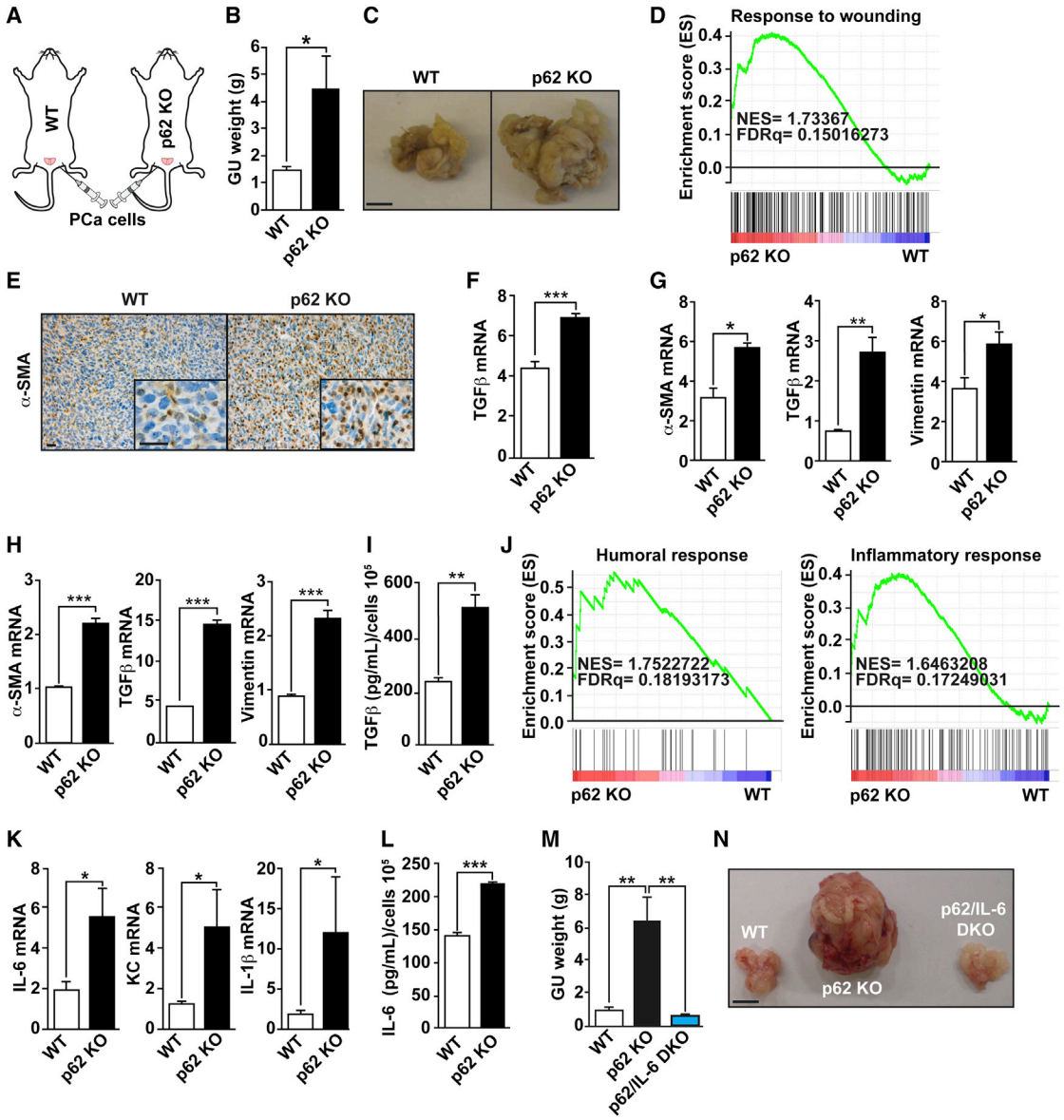

Figure 2. IL-6 Is Required for p62's Role in the Tumor Microenvironment

(A) Orthotopic injection of TRAMP-C2Re3 cells into the prostates of syngeneic WT and p62 KO mice. Orthotopic tumors were allowed to grow for two months.

(B and C) GU tract weight (B) and pictures (C) from (A); n = 5 or 6 mice per genotype. The scale bar represents 1 cm.

(D) "Response to wounding" GSEA plot of enrichment of gene expression in p62 KO orthotopic tumors.

(E) α-SMA staining of orthotopic tumors from WT and p62 KO mice. The scale bars represent 25 μm.

(F) RT-PCR of TGF-β in orthotopic tumors from WT and p62 KO mice (n = 3).

(G and H) RT-PCR of CAF markers (α-SMA, TGF-β, and vimentin) in FACS-sorted prostate stromal fraction from WT and p62 KO mice (G) and in WT and p62 KO prostate fibroblasts (H); n = 3.

(I) TGF-β production in prostate fibroblasts was determined by ELISA.

(J) GSEA plots of enrichment of gene expression in p62 KO orthotopic tumors.

(K) RT-PCR of inflammatory cytokines in orthotopic tumors of WT and p62 KO mice; n = 5 or 6 animals per group versus WT.

(L) IL-6 ELISA in fibroblasts.

(M and N) Orthotopic injection of TRAMP-C2Re3 cells into the prostates of mice of different genotypes (n = 5 or 6 mice). GU weights (M) and pictures (N). The scale bar represents 1 cm.

*p < 0.05, **p < 0.01, ***p < 0.001. Results are presented as mean ± SEM. See also Figure S2.

in the stroma. The two major sources of IL-6 in the tumor microenvironment are macrophages and stromal fibroblasts (Hanahan and Coussens, 2012). Notably, 3D organotypic culture experiments established that fibroblasts (Figures 3B and 3C), but not macrophages (Figure S3D), from p62 KO mice recapitulated the p62 KO phenotype in the orthotopic tissue grafting

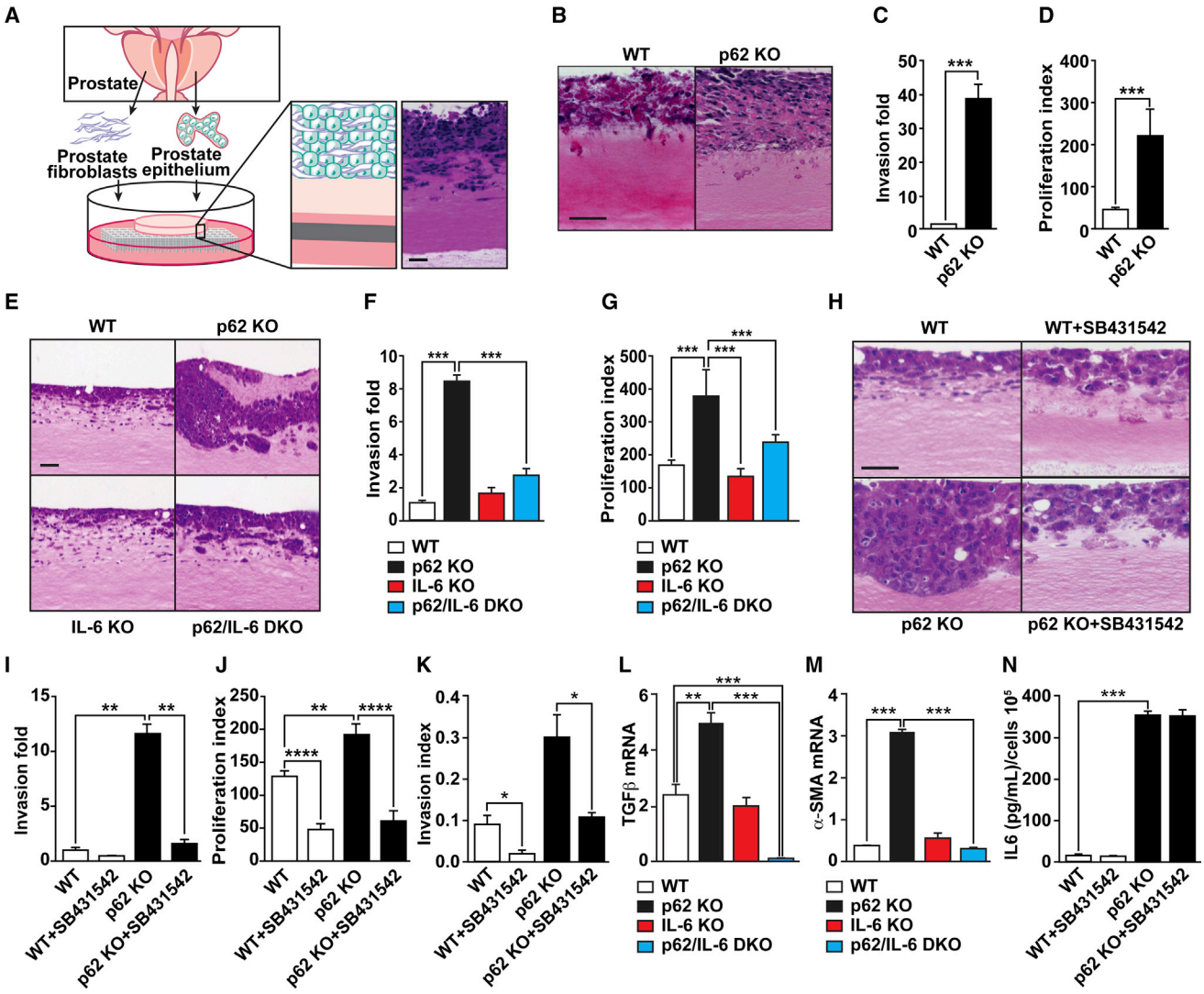

Figure 3. p62-Deficient Stroma-Mediated Invasion Is IL-6 and TGF-β Dependent

(A) Schematic representation of 3D organotypic cultures.

(B) H&E-stained sections of TRAMP-C2Re3 cells cultured in an organotypic system in the presence of primary prostate fibroblasts from WT and p62 KO mice.

(C and D) Quantification of PCa cell invasion (C) and proliferation index (D) of experiment shown in (B); n = 4.

(E) H&E staining of organotypic gels combining Myc-CaP cells with prostate fibroblasts from mice of different genotypes (n = 4).

(F and G) Quantification of PCa cell invasion (F) and proliferation index (G) of experiment shown in (E); n = 4.

(H) H&E staining of organotypic gels combining Myc-CaP cells with prostate fibroblasts from mice WT and p62 KO mice in the presence or absence of the TGF-β inhibitor SB431542 (10 μM).

(I and J) PCa cell invasion quantification (I) and proliferation index (J) of (H); n = 4.

(K) Invasion index determined by modified Boyden chamber assay with conditioned media from WT and p62 KO fibroblasts in the presence or absence of SB431542 (10 μM); n = 3.

(L and M) RT-PCR of TGF-β (L) and α-SMA (M) mRNA levels in fibroblasts of mice of different genotypes (n = 4).

(N) IL-6 production by WT and p62 KO fibroblasts in the presence or absence of the TGF-β inhibitor SB431542 (n = 4).

*p < 0.05, **p < 0.01, ***p < 0.001, ****p < 0.0001. Results are presented as mean ± SEM. The scale bars represent 100 μm. See also Figure S3.

experiment, and this effect was abolished when p62/IL-6 DKO fibroblasts were used in the 3D system (Figures 3E–3G). Furthermore, when TGF-β signaling was inhibited by incubating the organotypic cultures with the TGF-β inhibitor SB431542 (Inman et al., 2002), the protumorigenic phenotype of p62-deficient fibroblasts was reverted, consistent with the notion that TGF-β is important for the CAF phenotype and PCa proliferation (Figures 3H–3J). Likewise, the TGF-β inhibitor reverted the increased invasion index of PCa cells incubated with p62-deficient fibroblast conditioned medium in a Boyden chamber invasion assay (Figure 3K). Results shown in Figure S3E demonstrate the effectiveness of this inhibitor to block the TGF-β pathway. Moreover, the enhanced TGF-β production observed in the p62 KO fibroblasts, as well as that of α-SMA, was completely abrogated in

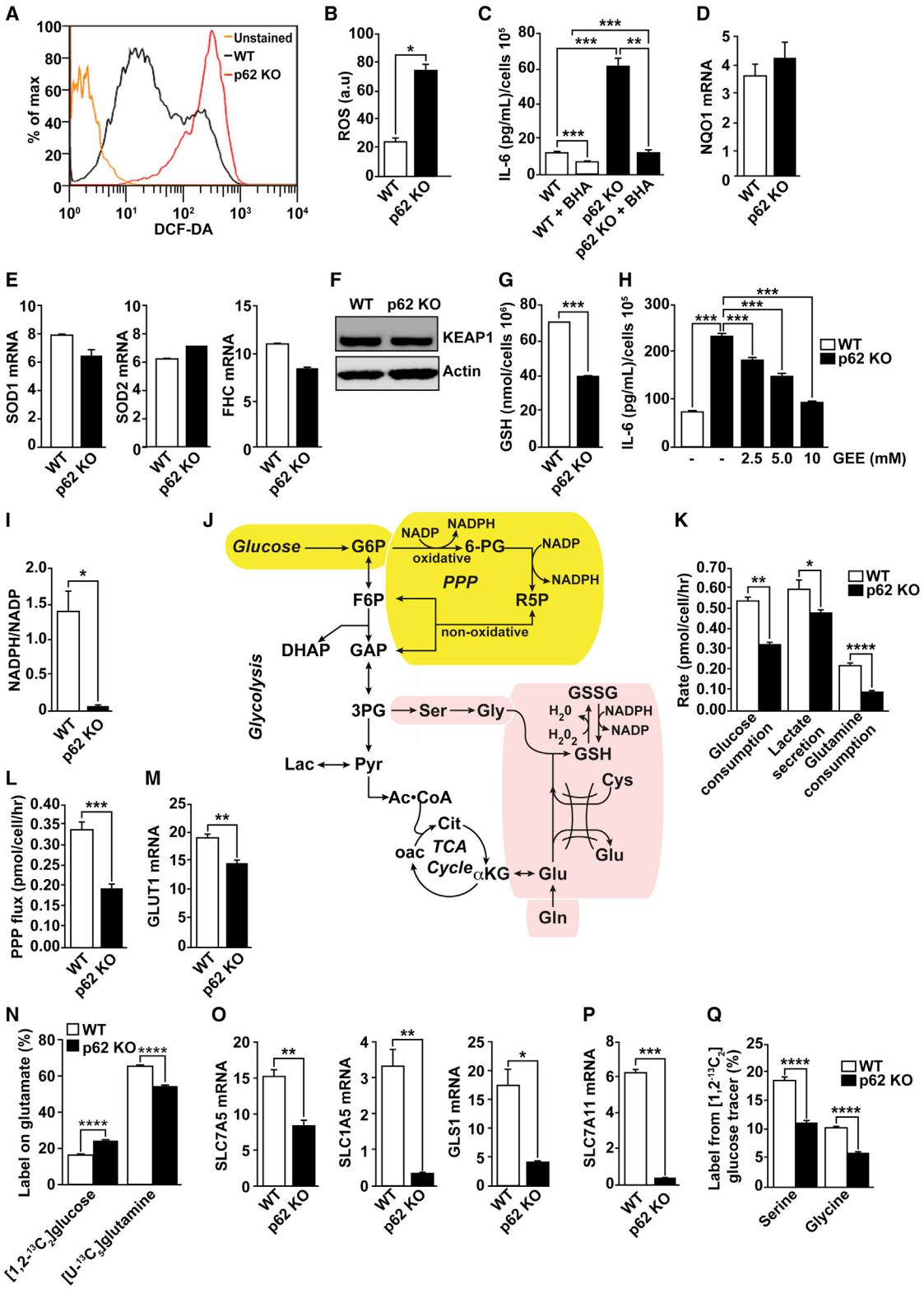

Figure 4. Metabolic Reprogramming in p62-Deficient Stroma

(A and B) Total intracellular levels of ROS in WT and p62 KO fibroblasts (A) and quantification (B); n = 4.

(C) IL-6 ELISA of WT and p62 KO fibroblasts treated with vehicle or the ROS scavenger BHA (100 μM) for 12 hr (n = 4).

(D and E) RT-PCR of NQO1 (D) and SOD1, SOD2, and FHC (E) mRNA levels in fibroblasts (n = 4).

(legend continued on next page)

the DKO fibroblasts (Figures 3L and 3M). Consistently, the knockdown of IL-6 in p62 KO fibroblasts impaired IL-6 secretion and, more important, also reverted TGF-β production and PCa invasion (Figures S3F–S3H). Furthermore, incubation of p62/IL-6 DKO fibroblasts with exogenously added IL-6 restored TGF-β levels to those of p62 KO cells as well as PCa invasion (Figure S3I and S3J). All this is consistent with a cell-autonomous role of the p62-IL-6 axis in the control of the CAF phenotype. However, incubation of p62 KO fibroblasts with the TGF-β signaling inhibitor SB431542 did not affect the overproduction of IL-6 in p62 KO fibroblasts (Figure 3N). These are important observations that establish a sequential p62/IL-6/TGF-β axis in the tumor fibroblastic compartment contributing to the control of epithelial tumorigenesis during PCa progression.

p62 Controls IL-6 Levels by Repressing Reactive Oxygen Species Production through Metabolic Reprogramming

We next sought to determine how p62 controls IL-6 production in fibroblastic stromal cells and whether the mechanisms mediating IL-6 production are relevant to stroma-driven tumorigenesis. It should be noted that p62 KO fibroblasts have increased levels of reactive oxygen species (ROS) (Figures 4A and 4B) and that the inhibition of ROS production (by the ROS scavenger butylated hydroxyanisole [BHA]) completely reverts the IL-6 hyperproduction phenotype (Figure 4C). This indicates that the mechanism whereby p62 represses IL-6 production in fibroblasts involves the control of ROS levels. It has previously been reported that p62 can activate NF-κB and NRF2 (Duran et al., 2008; Komatsu et al., 2010; Moscat and Diaz-Meco, 2009), which suggests that these molecules could play a role in the ability of p62 to repress ROS production and the subsequent activation of IL-6. The expression of critical detoxifying NF-κB- or NRF2-dependent genes (Figures 4D and 4E), as well as the levels of the NRF2 inhibitor Keap1 (Figure 4F), was not affected by the loss of p62 in fibroblasts. However, we found that p62 KO fibroblasts displayed lower levels of reduced glutathione (GSH) than the WT controls (Figure 4G). These are important observations because GSH is central to the control of ROS levels. In fact, treatment of p62 KO fibroblasts with the GSH analog GSH-reduced ethyl ester (GEE) reduced IL-6 to levels comparable with those of WT fibroblasts (Figure 4H). These results demonstrate that the loss of p62 results in lower GSH levels, thus promoting ROS accumulation, which is required for IL-6 overproduction in p62-deficient fibroblasts.

We observed a striking decrease in the reduced nicotinamide adenine dinucleotide phosphate (NADPH)/nicotinamide adenine dinucleotide phosphate (NADP) ratio in p62-deficient fibroblasts (Figure 4I). This ratio provides additional information on the cellular redox status, as the relative concentration of GSH versus oxidized GSH depends on the cellular content of NADPH. Glycolytic metabolism plays a critical role in maintaining NADPH production through the oxidative pentose phosphate pathway (PPP) (Figure 4J, yellow shading). Indeed, p62 KO cells exhibited decreased glucose uptake and lactate secretion (Figure 4K). This reduction in glycolytic rate resulted in decreased flux through the oxidative PPP, as determined by stable isotope tracing with [1,2-$^{13}C_2$]glucose (Figure 4L). These metabolic changes correlated with a reduction in GLUT1 levels in p62-deficient fibroblasts (Figure 4M), providing evidence that transcriptional changes associated with p62 loss influence metabolic flux.

Amino acids are critical for the production of GSH, a peptide composed of glutamate, cysteine, and glycine (Figure 4J, pink shading). Glutamine serves as an important precursor for glutamate, and loss of p62 in fibroblasts leads to lower glutamine consumption compared with WT cells (Figure 4K). We also observed a decrease in the direct conversion of [U-$^{13}C_5$] glutamine to glutamate in p62 KO fibroblasts, with a relative increase in the fraction of glutamate derived from [1,2-$^{13}C_2$]glucose (Figure 4N). In good agreement with these changes in glutamine metabolism, we observed reduced levels of the glutamine transporters SLC7A5 and SLC1A5, as well as glutaminase-1 (GLS1) (Figure 4O), a critical enzyme in the pathway that catalyzes the conversion of glutamine into glutamate (Figure 4J). Consistent with reduced levels of GSH, p62 KO fibroblasts also exhibit a dramatic reduction in the levels of SLC7A11, the xCT cystine/glutamate antiporter, which is the major driver of cystine uptake, a critical and rate-limiting step in the synthesis of GSH in several cell types, including fibroblasts (Figure 4P) (Bannai and Tateishi, 1986; Gout et al., 1997). Finally, we observed significant decreases in labeling of both serine and glycine from [1,2-$^{13}C_2$] glucose (Figure 4Q). Serine serves as a precursor to glycine and cysteine (when synthesized from methionine), so this decrease in label transfer provides evidence that there is less demand for GSH synthesis in p62-deficient cells. These results collectively demonstrate that loss of p62 in fibroblasts influences metabolic pathways controlling cellular redox, including NADPH production in the PPP and GSH synthesis.

p62 Is a Critical Regulator of c-Myc Levels

Previous data from other laboratories have established the critical role of c-Myc in the regulation of glutamine and glucose metabolism (Dang, 2012). We found significantly reduced levels of c-Myc in p62 KO fibroblasts as well as in WT fibroblasts in which p62 has been knocked down by small hairpin RNA (shRNA)

(F) Immunoblot analysis of KEAP1 in cell lysates from WT and p62 KO fibroblasts. Results are representative of three experiments.
(G) Cellular GSH levels in WT and p62 KO fibroblasts (n = 4).
(H) IL-6 ELISA of fibroblasts treated with increasing concentrations of the GSH analog GEE (n = 4).
(I) Cellular NADPH/NADP levels in WT and p62 KO fibroblasts (n = 4).
(J) Metabolic scheme depicting biosynthetic routes to NAPDH (yellow shading) and GSH (pink shading) from glucose and glutamine.
(K) Glucose consumption, lactate secretion, and glutamine consumption rates determined by spent medium analysis from WT and p62 KO fibroblasts (n = 3).
(L) PPP flux estimates from metabolic flux analysis in WT and p62 KO fibroblast cultures labeled with [1,2-$^{13}C_2$]glucose (n = 3).
(M) RT-PCR of GLUT1 mRNA (n = 4).
(N) Glutamate labeling in WT and p62 KO fibroblasts grown in either [1,2-$^{13}C_2$]glucose and unlabeled glutamine or [U-$^{13}C_5$]glutamine and unlabeled glucose (n = 3).
(O and P) RT-PCR of SLC7A5, SLC1A5, and GLS1 (O) and SLC7A11 (P) mRNA levels in WT and p62 KO fibroblasts (n = 3).
(Q) Labeling of serine and glycine from [1,2$^{13}C_2$]glucose (n = 3).
*p < 0.05, **p < 0.01, ***p < 0.001, ****p < 0.0001. Results are presented as mean ± SEM.

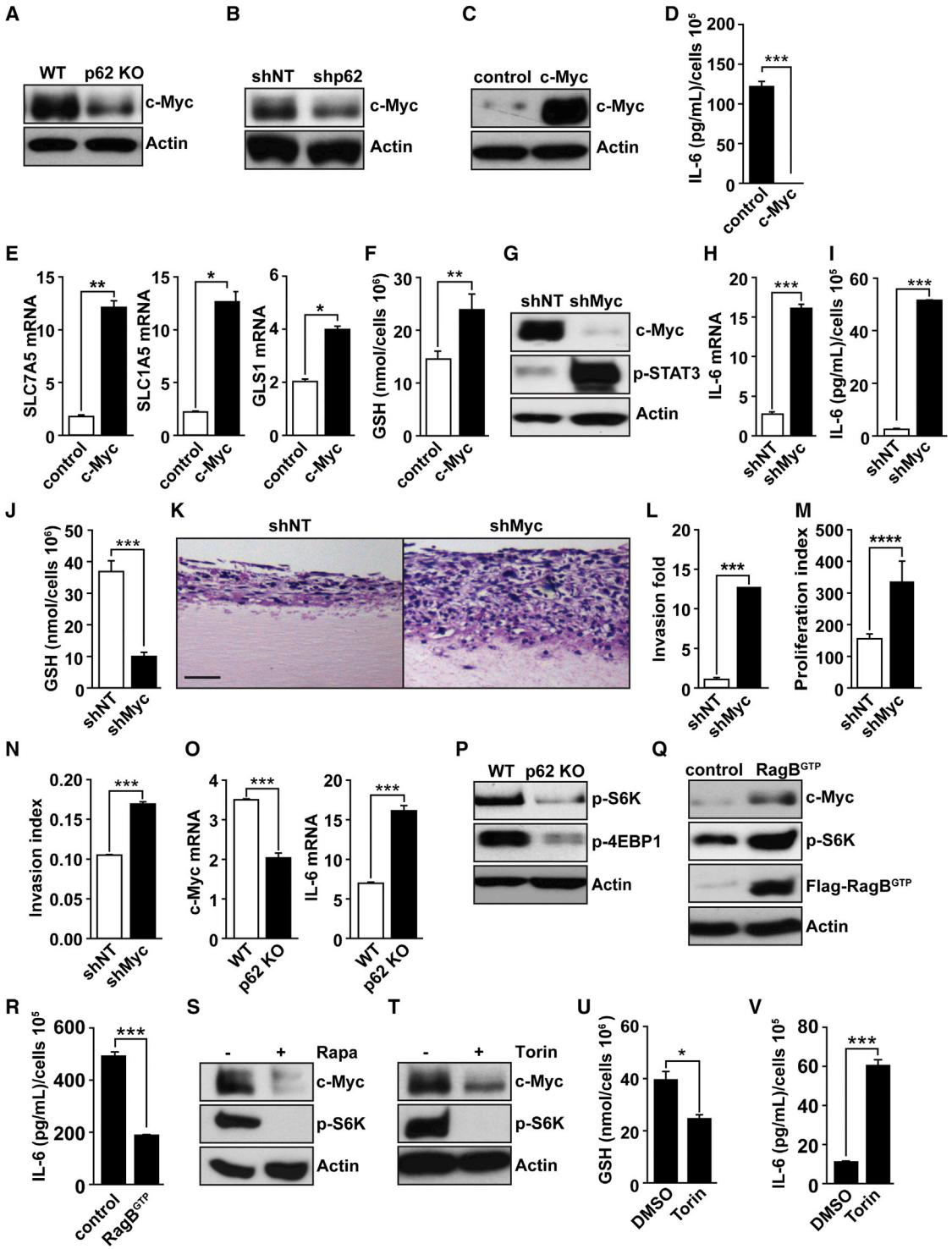

Figure 5. c-Myc-Mediated Metabolism in p62-Deficient Stroma

(A–C) Immunoblot analysis of c-Myc levels in WT and p62 KO fibroblasts (A), in WT fibroblasts lentivirally infected with shRNA nontargeted control (shNT) or shRNA specific for p62 (shp62) (B), and in p62 KO fibroblasts retrovirally infected with control vector (control) or with c-Myc expression vector (c-Myc) (C). Results are representative of three experiments.

(D) IL-6 ELISA in control and c-Myc cells (n = 4) as in (C).

(E) RT-PCR of SLC7A5, SLC1A5, and GLS1 mRNA in control and c-Myc cells (n = 3).

(F) Intracellular GSH levels in control and c-Myc cells (n = 3).

(G) Immunoblot analysis of c-Myc and p-STAT3 in WT fibroblasts infected with shNT or shRNA for c-Myc (shMyc).

(legend continued on next page)

(Figures 5A and 5B) and reductions in the levels of the key glutamine transporters SLC7A5 and SLC1A5, and GLS1 (Figure 4O), which are targets of c-Myc (Dang, 2012). Interestingly, ectopic expression of c-Myc in p62 KO fibroblasts (Figure 5C) reverted the p62-deficient phenotype in terms of IL-6 production (Figure 5D) and the levels of glutamine transporters and GLS1 (Figure 5E) and GSH (Figure 5F). On the contrary, c-Myc knockdown in WT fibroblasts (Figure 5G) resulted in increased IL-6 production at the mRNA and protein levels (Figures 5H and 5I). c-Myc knockdown in fibroblasts led to decreased levels of GSH (Figure 5J), as well as enhanced PCa cell invasion and proliferation in organotypic cell cultures (Figures 5K–5M). Also, the knockdown of c-Myc in fibroblasts resulted in increased PCa cell invasion index in a Boyden chamber assay (Figure 5N). Of note, this cause-and-effect correlation between p62 deficiency, c-Myc expression, and IL-6 production was also found in FACS-isolated prostate stromal cells from WT and p62 KO mice (Figure 5O). Collectively these results demonstrate that p62 repression of c-Myc expression in the stroma fibroblasts accounts for its tumor suppressive role in PCa.

IL-6 Is Regulated by a p62/mTORC1/c-Myc Cascade

Consistent with previously published observation (Duran et al., 2011), we found that p62 KO cells displayed reduced mTORC1 activity (Figure 5P). We hypothesized that the reduction in c-Myc levels found in p62 KO fibroblasts could be the consequence of mTORC1 inhibition. Importantly, we rescued c-Myc inhibition in p62 KO fibroblasts by expressing a permanently active mutant of the small-guanosine triphosphatase RagB, which is a critical activator of mTORC1 (Figure 5Q). IL-6 levels were likewise reduced under these conditions (Figure 5R). These results demonstrate that reduced mTORC1 activity in p62 KO fibroblasts accounts for the low levels of c-Myc and the subsequent increase in IL-6 production in these mutant cells. Treatment of WT fibroblasts with rapamycin or Torin, two different inhibitors of mTORC1, effectively reduced c-Myc levels (Figures 5S and 5T), promoting a significant reduction in GSH levels (Figure 5U) and a concomitant increase in IL-6 production (Figure 5V). Therefore, p62's ability to regulate mTORC1 in the stroma is essential for its control of the c-Myc/GSH/IL-6 axis.

p62 KO Mice Develop Prostate Hyperplasia and Prostatic Intraepithelial Neoplasia upon Aging

On the basis of these results, we hypothesized that the loss of p62 at an organismal level, which would include both the prostate stroma and epithelium, might be sufficient to drive prostate epithelium toward neoplasia. We characterized the prostates of p62 KO mice by histological analysis, which revealed no abnormalities in development or morphology at early stages. However, at 9 months of age, prostates from p62 KO mice developed hyperplasia, with a concomitant increase in Ki67 staining (Figures 6A and 6B). These lesions progressed to prostatic intraepithelial neoplasia (PIN) at 1 year of age (Figure 6C). This indicated that, whereas in xenograft experiments PCa epithelial cells with reduced p62 displayed inhibited tumorigenesis (Duran et al., 2011), the total loss of p62 in vivo promoted prostate epithelial cell growth. These observations are in good agreement with our model whereby p62 in the stromal fibroblasts normally acts as a tumor suppressor, and the total KO of p62 results in p62-deficient stromal fibroblasts that drive the prostate epithelium to a malignancy-prone state. To further test this hypothesis, we crossed total p62 KO mice with two well-established mouse models of PCa ($PTEN^{+/-}$ and $TRAMP^{+}$) (Di Cristofano et al., 1998; Greenberg et al., 1995) and asked whether total ablation of p62 inhibited or promoted prostate tumor development. Figures 6D and 6E show hematoxylin and eosin (H&E) analyses of $PTEN^{+/-}$/p62 KO prostrates demonstrating an increase in the percentage of glands with high-grade PIN at the age of 6 months. Furthermore, $TRAMP^{+}$/p62 KO mice had reduced survival (Figure 6F), increased percentages of poorly differentiated adenocarcinoma (Figure 6G) and neuroendocrine tumors (Figure 6H), as well as a larger number of metastases (Figure 6I), of which a higher percentage were in the liver (Figure 6J). Consistent with our model, prostate fibroblasts from $PTEN^{+/-}$/p62 KO mice showed increased IL-6 and reduced c-Myc expression compared with those from p62-proficent $PTEN^{+/-}$ mice (Figures S4A–S4C). Interestingly, immunohistochemical analysis of prostates from $PTEN^{+/-}$ mice confirmed reduced expression of p62 in the stromal compartment compared with those from WT mice (Figure S4D). To further support the role of p62 deficiency in the stroma in driving tumorigenesis in vivo, we coinjected syngeneic PCa cells (TRAMP-C2Re3) with WT or p62 KO fibroblasts and assessed the effect that fibroblasts exert on tumor growth. Tumors coinjected with p62 KO fibroblasts grew significantly faster and were larger than tumors in mice injected with WT fibroblasts, consistent with the cell-autonomous tumor-promoting activity of p62-deficient fibroblasts on epithelial PCa cells (Figures 6K and 6L). In agreement with this, bromodeoxyuridine (BrdU) incorporation was increased in the p62 KO fibroblast-driven tumors (Figures 6M and 6N).

(H and I) RT-PCR of IL-6 mRNA (H) and IL-6 ELISA (I) in the same cells (n = 3) as in (G).
(J) Quantification of intracellular GSH levels in WT shNT and shMyc cells (n = 3).
(K) H&E-stained organotypic gels of TRAMP-C2Re3 cells with shNT or shMyc fibroblasts. The scale bar represents 100 μm.
(L and M) Quantification of PCa cell invasion (L) and proliferation index (M) of experiment shown in (K).
(N) Invasion index determined by modified Boyden chamber assay of Myc-CaP cells cocultured with shNT and shMyc fibroblasts.
(O) RT-PCR of c-Myc and IL-6 mRNA levels in FACS-isolated prostate stromal cells from WT and p62 KO mice (n = 3).
(P) Immunoblot analysis with the indicated antibodies of cell lysates of WT and p62 KO fibroblasts.
(Q) Immunoblot analysis for the specified proteins of cell lysates from p62 KO fibroblasts retrovirally infected with control vector (control) or FLAG-$RagB^{GTP}$ expression vector ($RagB^{GTP}$). Results are representative of three experiments.
(R) IL-6 ELISA (n = 3) in cells shown in (Q).
(S and T) Immunoblot analysis of c-Myc and p-S6K in fibroblasts treated with rapamycin (S) or Torin1 (T) for 12 hr.
(U) Intracellular GSH levels in fibroblasts treated with Torin1.
(V) IL-6 ELISA in fibroblasts treated with Torin1 (n = 3).
*p < 0.05, **p < 0.01, ***p < 0.001, ****p < 0.0001. Results are presented as mean ± SEM.

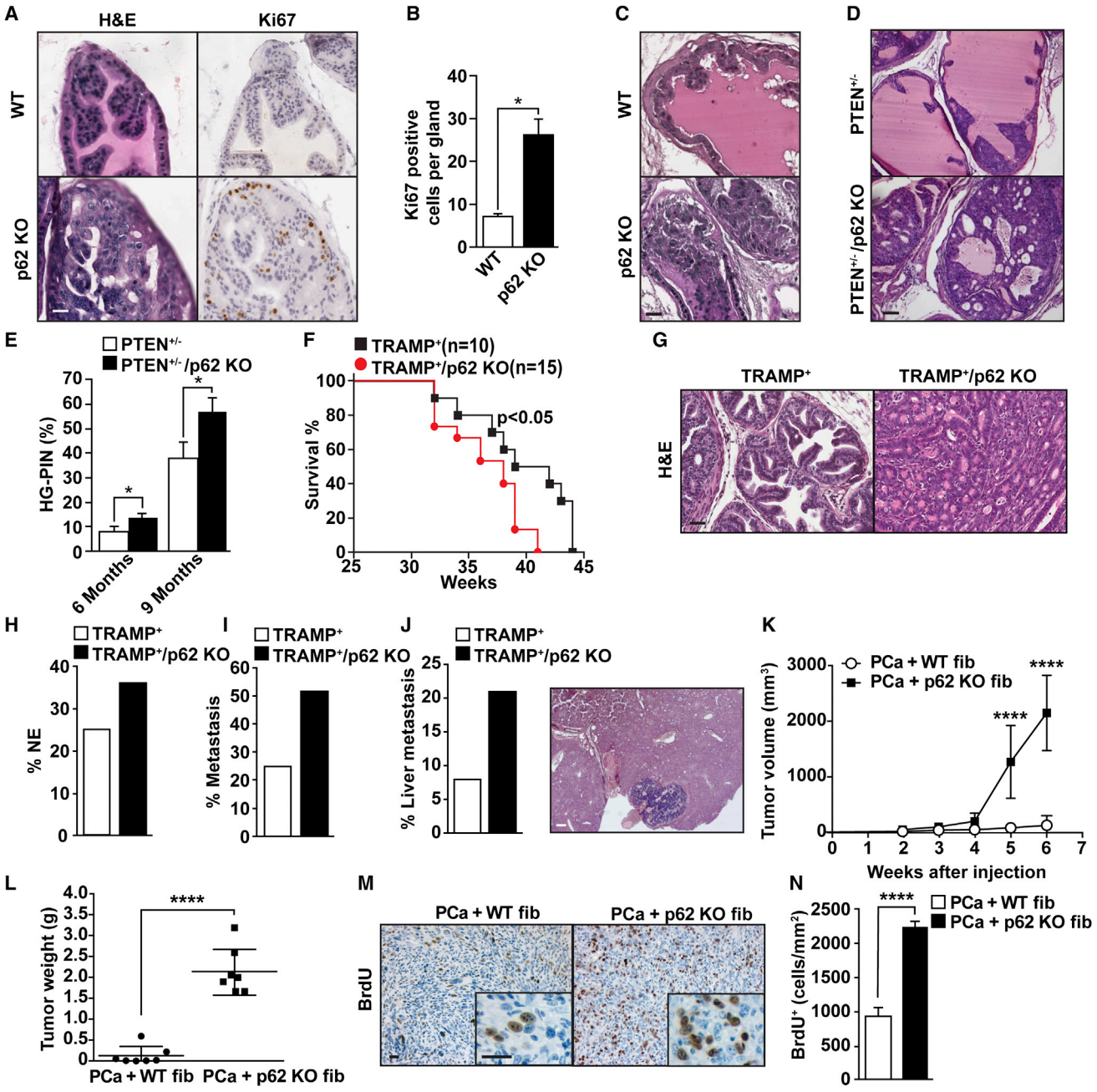

Figure 6. p62 Deficiency Accelerates Prostate Tumor Progression in Different Mouse Models of Prostate Cancer

(A) Hyperplasia in the prostatic anterior lobe of p62 KO mice. H&E and Ki67 staining of prostates from 9-month-old WT and p62 KO mice (n = 5).

(B) Quantification of Ki67-positive cells in the prostate sections shown in (A). Results are the means ± SD of counts from 10 different fields per mouse (n = 5).

(C) PIN in the dorsolateral lobes of prostates from 12-month-old p62 KO mice.

(D) Representative examples of H&E staining of dorsolateral lobes of prostates from $PTEN^{+/-}$ and $PTEN^{+/-}$/p62 KO mice at 6 months of age (n = 5).

(E) Percentage of glands with HG-PIN (n = 5 mice).

(F) Kaplan-Meier survival curve of $TRAMP^{+}$ mice (n = 10), compared with $TRAMP^{+}$/p62 KO mice (n = 15).

(G) Representative H&E staining of mouse prostate sections from $TRAMP^{+}$ and $TRAMP^{+}$/p62 KO mice (n = 10).

(H) Incidence of neuroendocrine tumors in $TRAMP^{+}$ (n = 12) and $TRAMP^{+}$/p62 KO mice (n = 19).

(I and J) Incidence of metastasis (I) and liver metastasis (J) in $TRAMP^{+}$ compared with $TRAMP^{+}$/p62 KO mice.

(K–M) Coinjection of syngeneic TRAMPC2-Re3 PCa cells with either WT or p62 KO fibroblasts in C57BL/6 mice. (K) Tumor volume assessed at different time points after injection (n = 7 mice). (L) Tumor weight at 6 weeks after injection (n = 7 mice). (M) BrdU staining in tumor sections.

(N) Quantification of BrdU positive cells of (M).

Results are presented as mean ± SEM (n = 10). *p < 0.05, ****p < 0.001. The scale bars represent 25 μm. See also Figure S4.

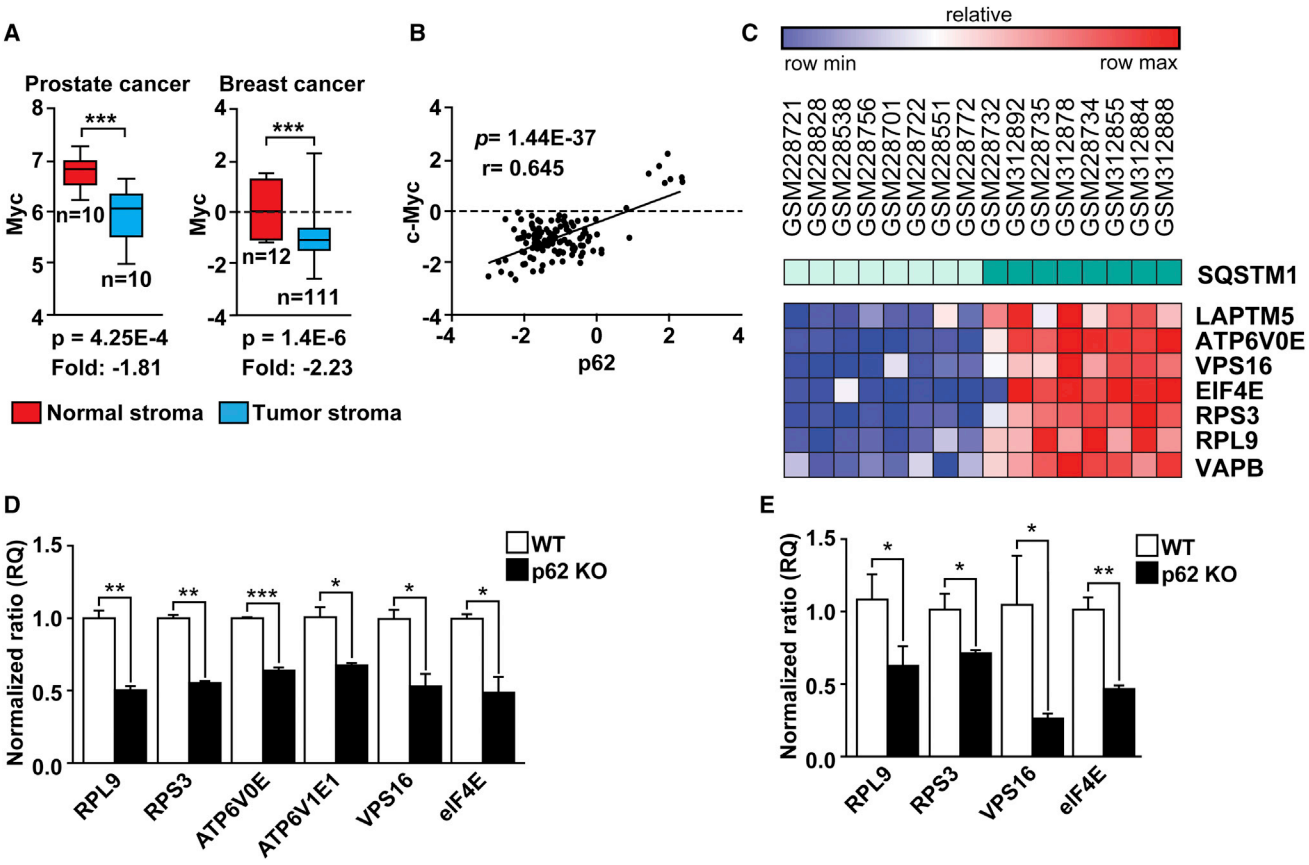

Figure 7. The p62-Myc-mTORC1 Cassette Is Downregulated in Prostate Tumor-Associated Stroma in Human Samples

(A) Myc levels are downregulated in the tumor stroma of human tissue samples. Data were collated from public data sets of gene expression in tumor stroma in several human cancers: GSE34312 (prostate cancer) and GSE9014 (breast cancer). The p value, fold change of expression, and size of the sample (n) for each study are indicated in the corresponding panels.

(B) Positive correlation between p62 and Myc levels in the stroma.

(C) Heatmap of mTORC1 signature selected from p62 neighboring genes in human stroma. p62 levels are indicated as SQSTM1.

(D and E) RT-PCR analysis of mTORC1 genes in WT and p62 KO fibroblasts (D) and in FACS sorted mouse prostate stromal fraction (E).

*p < 0.05, **p < 0.01, ***p < 0.001. Results are presented as mean ± SEM (n = 3). See also Figure S5.

p62/mTORC1/c-Myc Connection in Human Cancer Stroma

To determine whether the identified link between p62 and c-Myc through mTORC1 has relevance to the role of the stroma in human cancer, we used bioinformatics to analyze c-Myc transcript levels in two sets of human gene-expression arrays from prostate and breast cancer stroma. Stroma of human tumors displayed reduced levels of c-Myc (Figure 7A), and there was a statistically significant correlation between c-Myc and p62 expression in tumor stroma (Figure 7B), emphasizing the clinical relevance of the p62-Myc connection in the stroma. To further explore the link between p62 and mTORC1 in the tumor stroma of human cancers, we identified expression neighbors of p62. We developed this gene signature by using the human cancer stroma data set shown in Figure 7A, in which we classified tumors on the basis of p62 expression levels and selected for analysis only those samples in the top and bottom 25%. Interestingly, this analysis revealed a statistically significant correlation between p62 expression and that of genes previously reported to be controlled by mTORC1 activity (Figure 7C; Figure S5) (Peña-Llopis et al., 2011). We determined the expression levels of a selection of these genes by RT-PCR and found that their expression was reduced in p62 KO fibroblasts compared with WT (Figure 7D). The same results were obtained when these were analyzed in prostate stromal cell preparations from p62 KO and WT mice (Figure 7E). Furthermore, we found a clear statistically significant correlation between p62 expression and that of these genes in human cancer stroma (Figures S5B–S5H). Altogether, these results demonstrate that the p62/mTORC1/c-Myc connection is not only relevant in the mouse prostate stroma but it is also important in human cancer stroma.

DISCUSSION

Tumorigenesis is a slow process that is initiated by the successive accumulation of genetic and epigenetic changes that result in the activation of cell growth and survival genes and the inactivation of tumor suppressors (Hanahan and Weinberg, 2011). However, for tumor development to take place, initiation is not sufficient. Other signals are required to drive tumor promotion

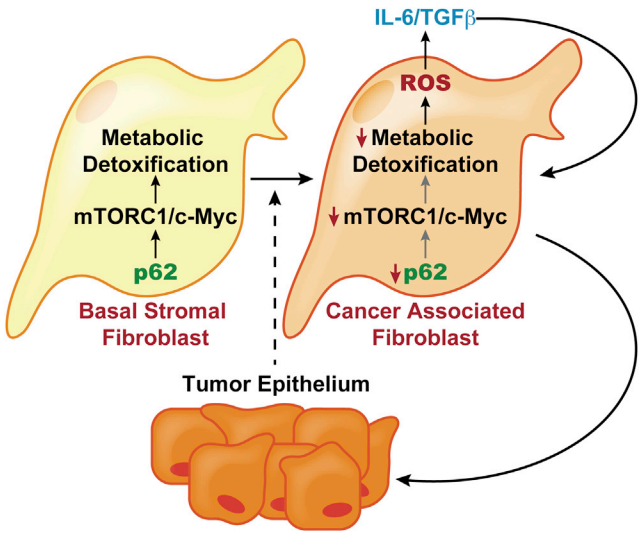

Figure 8. Stromal Activation by p62 Deficiency in Cancer
Tumor epithelium promotes the downregulation of p62 in stromal fibroblasts, leading to reduced mTORC1 activity and c-Myc expression, which results in impaired metabolic detoxification and the subsequent release of ROS and IL-6. An autocrine pathway promotes TGF-β and the induction of CAF phenotype, which further increases epithelial invasion and tumorigenesis.

and progression and the development of the fully malignant stage. The progression phase is most likely orchestrated via the tumor microenvironment by nonepithelial cells in which metabolic stress and inflammation create an environment in which epithelial tumor-derived cells propagate and acquire more aggressive phenotypes (Hanahan and Coussens, 2012; Hanahan and Weinberg, 2011). Immune cells, such as tumor-associated macrophages, are among the cell types in the tumor microenvironment that contribute to inflammation (Coussens and Werb, 2002; Johansson et al., 2008). On the other hand, a crosstalk between metabolic pathways in the stromal and epithelial compartments of the tumor may drive the survival and growth of epithelial cancer cells (Lisanti et al., 2013). However, it has not been thoroughly investigated whether metabolic reprogramming in the stromal cells of the tumor microenvironment exerts any control over inflammation and the malignant characteristics of the transformed epithelium.

Here we demonstrate that the inactivation of mTORC1 in p62-deficient stromal fibroblasts results in metabolic reprogramming through c-Myc inactivation (Figure 8). This reprogramming leads to increased levels of IL-6, which promotes epithelial cell invasion and proliferation. Therefore, because of its regulation of mTORC1, p62 emerges as a tumor suppressor that acts by regulating c-Myc and thus inducing an inflammatory response. These results are in marked contrast to the role played by p62 and mTORC1 in epithelial cancer cells. That is, we have recently demonstrated that p62 inactivation in PCa and lung adenocarcinoma epithelial cells inhibits the proliferation and tumorigenic properties of these cells and correlates with decreased mTORC1 activation. Moreover, the increased IL-6 phenotype can be reverted by expression of a permanently active mutant of the mTORC1 activator RagB. This has important implications from a therapeutic point of view because inhibition of p62 and/or mTORC1 may result in opposite effects in the stroma and the epithelium of the tumor, thus reducing the efficacy of broadly applied mTORC1-based chemotherapeutic approaches. In this regard, these results are reminiscent of the dual role that mTORC1 might play as a regulator of autophagy, which can have a tumor-suppressing or a tumor-promoting effect, depending of the stage of the tumor (Guo et al., 2013; Levine and Kroemer, 2008), and also on whether the manipulation takes place in the epithelium or in the stroma (Lisanti et al., 2013). Our data using KO mice clearly reveal that p62 deficiency creates a protumorigenic environment for p62-proficient PCa cells in orthotopic experiments and also show that, even under normal conditions, it drives PIN formation in the endogenous epithelium in the absence of any other induced mutations. Furthermore, in two PCa models, the lack of p62 at an organismal level results in increased tumorigenesis, despite the fact that p62 is absent not only in the stroma but also in the transformed epithelium. These results are very important because they demonstrate that even though p62 is required for epithelial cancer cells to proliferate in vitro and in xenografts (Duran et al., 2011), the p62-deficient tumor microenvironment overrides the requirement for p62 in the epithelium. Our in vitro and in vivo findings establish that increased IL-6 levels generated by stromal fibroblasts are a critical event in that process. Therefore, it can be predicted that total ablation of p62 at an organismal level, either genetically or pharmacologically, may increase tumorigenesis, rather than inhibiting it, depending on the contribution of the stroma and the ability of p62 deficiency to reprogram stromal metabolism to generate ROS and inflammation. Our data shown here demonstrate that this is the case in prostate tumorigenesis and suggest that it could be a relevant mechanism in other tumor types as well. The proinflammatory microenvironment in the p62-deficient stroma results in a CAF-activated phenotype that is maintained by stromal TGF-β production. This is consistent with previous results in colon cancer demonstrating that a TGF-β-activated tumor microenvironment is critical for fully aggressive cancer cells to metastasize (Calon et al., 2012).

Metabolic reprogramming in cancer is emerging as a central process in tumor cell survival and growth (DeBerardinis and Thompson, 2012; Metallo and Vander Heiden, 2013; Vander Heiden, 2013). The so-called Warburg effect supports the importance of an atypical glucose metabolism tailored to the cancer cell's need for efficient anabolic utilization of nutrients (Vander Heiden et al., 2009). More recently, different types of reprogramming events have been unveiled that constitute specific responses of the tumor cell to a nutrient-deficient environment. These include the metabolism of serine or the utilization of the PPP to alleviate oxidative stress conditions during tumorigenesis (Locasale, 2013; Ma et al., 2013; Possemato et al., 2011; Vander Heiden et al., 2010). In the current study, we show that metabolic reprogramming triggered by p62 deficiency in the tumor stroma is critical for the creation of a protumorigenic inflammatory environment driven by IL-6. Moreover, we have shown that this involves an mTORC1/c-Myc/ROS cascade that is controlled by p62. In this regard, previous results from our and other laboratories have shown that p62 represses ROS by inducing the activation of NF-κB- or NRF2-dependent detoxifying molecules (Duran et al., 2008; Komatsu et al., 2010; Ling et al., 2012). Surprisingly, neither of these two transcription factors nor Keap1

levels were affected in p62-deficient stromal fibroblasts, indicating that p62 may use diverse cascades in different cellular compartments of the tumor. Interestingly, our previous data demonstrate that under conditions of Ras-induced transformation, p62 deficiency leads to increased cell death and reduced tumorigenesis due to enhanced ROS production (Duran et al., 2008). In contrast, we show here that the enhanced ROS observed in the untransformed stromal fibroblasts does not result in increased cell death but rather in the creation of a proinflammatory phenotype. The main conclusion of these results is that increased ROS production induced by p62 deficiency has different outcomes depending on the cell type and the mechanisms whereby ROS is produced. The outcome also depends on whether or not the levels of ROS are high enough to engage a c-Jun N-terminal kinase-driven cell-death pathway, as found in the Ras-tumor cell, as opposed to increased IL-6 production and a protumorigenic effect on epithelial cells, as we demonstrated in the stromal nontransformed fibroblasts.

Importantly, we were able to show that the implication of the p62/mTORC1/c-Myc cascade is relevant not only in mouse model systems but also in human samples, in which this pathway is inactivated in the tumor stroma. Therefore, our findings support a more comprehensive approach when devising therapeutic strategies in cancer, which should take into account not only the altered pathways in the transformed epithelial compartment but also how the inhibition of these cascades might affect the surrounding stroma. Our observations suggest that pharmacological inhibition of IL-6 and/or TGF-β to target stromal activation could be beneficial in combination with epithelial-targeted therapies.

EXPERIMENTAL PROCEDURES

Mice

WT, p62 KO, PTEN$^{+/-}$, and TRAMP^{+} mice were previously described (Durán et al., 2004; Di Cristofano et al., 1998; Greenberg et al., 1995). All mouse strains were generated in a C57BL/6 background. All mice were born and maintained under pathogen-free conditions. All genotyping was done by PCR. Mice were sacrificed and genitourinary (GU) sections were dissected. Mice were injected with 5-bromo-2′-deoxyuridine intraperitoneally and sacrificed 2 hr after injection. Animal handling and experimental procedures conformed to institutional guidelines (Sanford-Burnham Medical Research Institute Institutional Animal Care and Use Committee).

Cell Lysis and Western Immunoblotting

Cells were rinsed once with ice-cold PBS and lysed in radioimmunoprecipitation assay buffer (1 × PBS, 1% Nonidet P-40, 0.5% sodium deoxycholate, 0.1% SDS, 1 mM phenyl methyl sulfonyl fluoride, and protease inhibitors). Cell extracts were denatured, subjected to 8% to 14% SDS-PAGE, transferred to nitrocellulose-enhanced chemiluminescence membranes (GE Healthcare), and immunoblotted with the specific antibodies. Chemiluminescence was used to detect the proteins (Thermo Scientific).

Statistical Analysis

Significant differences between groups were determined using Student's t test. Scoring of immunostaining of human prostate tissue microarrays was analyzed using Fisher's exact test. The significance level for statistical testing was set at $p < 0.05$.

ACCESSION NUMBERS

The Gene Expression Omnibus accession number for the microarray data reported in this paper is GSE55587.

SUPPLEMENTAL INFORMATION

Supplemental Information includes Supplemental Experimental Procedures and five figures and can be found with this article online at http://dx.doi.org/10.1016/j.ccr.2014.05.004.

AUTHOR CONTRIBUTIONS

T.V., J.Y.K., S.A.-B. and A.D. performed experiments. J.M.-P. and M.R.-C. performed bioinformatics analysis. E.A.C. provided pathologist expertise for histological analysis. C.S.A. and T.V. performed the metabolic experiments. C.M.M., M.D.M., and J.M. designed and analyzed metabolic data. M.D.M. and J.M conceived and supervised the project with equal contribution. M.D.M. and J.M. wrote the manuscript with assistance from all the authors.

ACKNOWLEDGMENTS

This work was funded by grants R01CA132847 (J.M.), R01CA172025 (J.M.), R01CA134530 (M.T.D.-M.), and 5P30CA030199 (M.T.D-M. and J.M.) from the NIH. Additional support was provided by grants W81XWH-13-1-0353 (M.T.D-M.), W81XWH-13-1-0354 (J.M.), and W81XWH-13-1-0105 (C.M.M.) from the U.S. Department of Defense. We thank Maryellen Daston for editing this manuscript; Diantha LaVine for the artwork; and Tomoko Yajima, Tom Hudson, Jessica Leung, and the personnel of the Cancer Metabolism, Flow Cytometry, Cell Imaging, Animal Facility, Histology, Functional Genomics and Viral Vectors Shared Resources at the Sanford-Burnham Medical Research Institute for technical assistance. We thank Neil Bhowmick for assistance in the preparation of prostate fibroblasts.

Received: December 24, 2013
Revised: March 17, 2014
Accepted: May 7, 2014
Published: July 3, 2014

REFERENCES

Ammirante, M., Luo, J.L., Grivennikov, S., Nedospasov, S., and Karin, M. (2010). B-cell-derived lymphotoxin promotes castration-resistant prostate cancer. Nature *464*, 302–305.

Azevedo, A., Cunha, V., Teixeira, A.L., and Medeiros, R. (2011). IL-6/IL-6R as a potential key signaling pathway in prostate cancer development. World J. Clin. Oncol. *2*, 384–396.

Bannai, S., and Tateishi, N. (1986). Role of membrane transport in metabolism and function of glutathione in mammals. J. Membr. Biol. *89*, 1–8.

Barron, D.A., and Rowley, D.R. (2012). The reactive stroma microenvironment and prostate cancer progression. Endocr. Relat. Cancer *19*, R187–R204.

Bissell, M.J., and Radisky, D. (2001). Putting tumours in context. Nat. Rev. Cancer *1*, 46–54.

Calon, A., Espinet, E., Palomo-Ponce, S., Tauriello, D.V., Iglesias, M., Céspedes, M.V., Sevillano, M., Nadal, C., Jung, P., Zhang, X.H., et al. (2012). Dependency of colorectal cancer on a TGF-β-driven program in stromal cells for metastasis initiation. Cancer Cell *22*, 571–584.

Coussens, L.M., and Werb, Z. (2002). Inflammation and cancer. Nature *420*, 860–867.

Dang, C.V. (2012). MYC on the path to cancer. Cell *149*, 22–35.

De Marzo, A.M., Platz, E.A., Sutcliffe, S., Xu, J., Grönberg, H., Drake, C.G., Nakai, Y., Isaacs, W.B., and Nelson, W.G. (2007). Inflammation in prostate carcinogenesis. Nat. Rev. Cancer *7*, 256–269.

DeBerardinis, R.J., and Thompson, C.B. (2012). Cellular metabolism and disease: what do metabolic outliers teach us? Cell *148*, 1132–1144.

Di Cristofano, A., Pesce, B., Cordon-Cardo, C., and Pandolfi, P.P. (1998). Pten is essential for embryonic development and tumour suppression. Nat. Genet. *19*, 348–355.

Diaz-Meco, M.T., and Moscat, J. (2012). The atypical PKCs in inflammation: NF-κB and beyond. Immunol. Rev. *246*, 154–167.

Durán, A., Serrano, M., Leitges, M., Flores, J.M., Picard, S., Brown, J.P., Moscat, J., and Diaz-Meco, M.T. (2004). The atypical PKC-interacting protein p62 is an important mediator of RANK-activated osteoclastogenesis. Dev. Cell *6*, 303–309.

Duran, A., Linares, J.F., Galvez, A.S., Wikenheiser, K., Flores, J.M., Diaz-Meco, M.T., and Moscat, J. (2008). The signaling adaptor p62 is an important NF-kappaB mediator in tumorigenesis. Cancer Cell *13*, 343–354.

Duran, A., Amanchy, R., Linares, J.F., Joshi, J., Abu-Baker, S., Porollo, A., Hansen, M., Moscat, J., and Diaz-Meco, M.T. (2011). p62 is a key regulator of nutrient sensing in the mTORC1 pathway. Mol. Cell *44*, 134–146.

Erez, N., Truitt, M., Olson, P., Arron, S.T., and Hanahan, D. (2010). Cancer-associated fibroblasts are activated in incipient neoplasia to orchestrate tumor-promoting inflammation in an NF-kappaB-dependent manner. Cancer Cell *17*, 135–147.

Franco, O.E., and Hayward, S.W. (2012). Targeting the tumor stroma as a novel therapeutic approach for prostate cancer. Adv. Pharmacol. *65*, 267–313.

Gaggioli, C., Hooper, S., Hidalgo-Carcedo, C., Grosse, R., Marshall, J.F., Harrington, K., and Sahai, E. (2007). Fibroblast-led collective invasion of carcinoma cells with differing roles for RhoGTPases in leading and following cells. Nat. Cell Biol. *9*, 1392–1400.

Galavotti, S., Bartesaghi, S., Faccenda, D., Shaked-Rabi, M., Sanzone, S., McEvoy, A., Dinsdale, D., Condorelli, F., Brandner, S., Campanella, M., et al. (2013). The autophagy-associated factors DRAM1 and p62 regulate cell migration and invasion in glioblastoma stem cells. Oncogene *32*, 699–712.

Gout, P.W., Kang, Y.J., Buckley, D.J., Bruchovsky, N., and Buckley, A.R. (1997). Increased cystine uptake capability associated with malignant progression of Nb2 lymphoma cells. Leukemia *11*, 1329–1337.

Greenberg, N.M., DeMayo, F., Finegold, M.J., Medina, D., Tilley, W.D., Aspinall, J.O., Cunha, G.R., Donjacour, A.A., Matusik, R.J., and Rosen, J.M. (1995). Prostate cancer in a transgenic mouse. Proc. Natl. Acad. Sci. USA *92*, 3439–3443.

Grivennikov, S.I., Greten, F.R., and Karin, M. (2010). Immunity, inflammation, and cancer. Cell *140*, 883–899.

Guo, Y., Xu, F., Lu, T., Duan, Z., and Zhang, Z. (2012). Interleukin-6 signaling pathway in targeted therapy for cancer. Cancer Treat. Rev. *38*, 904–910.

Guo, J.Y., Xia, B., and White, E. (2013). Autophagy-mediated tumor promotion. Cell *155*, 1216–1219.

Hanahan, D., and Weinberg, R.A. (2011). Hallmarks of cancer: the next generation. Cell *144*, 646–674.

Hanahan, D., and Coussens, L.M. (2012). Accessories to the crime: functions of cells recruited to the tumor microenvironment. Cancer Cell *21*, 309–322.

Inami, Y., Waguri, S., Sakamoto, A., Kouno, T., Nakada, K., Hino, O., Watanabe, S., Ando, J., Iwadate, M., Yamamoto, M., et al. (2011). Persistent activation of Nrf2 through p62 in hepatocellular carcinoma cells. J. Cell Biol. *193*, 275–284.

Inman, G.J., Nicolás, F.J., Callahan, J.F., Harling, J.D., Gaster, L.M., Reith, A.D., Laping, N.J., and Hill, C.S. (2002). SB-431542 is a potent and specific inhibitor of transforming growth factor-beta superfamily type I activin receptor-like kinase (ALK) receptors ALK4, ALK5, and ALK7. Mol. Pharmacol. *62*, 65–74.

Inoue, D., Suzuki, T., Mitsuishi, Y., Miki, Y., Suzuki, S., Sugawara, S., Watanabe, M., Sakurada, A., Endo, C., Uruno, A., et al. (2012). Accumulation of p62/SQSTM1 is associated with poor prognosis in patients with lung adenocarcinoma. Cancer Sci. *103*, 760–766.

Johansson, M., Denardo, D.G., and Coussens, L.M. (2008). Polarized immune responses differentially regulate cancer development. Immunol. Rev. *222*, 145–154.

Kim, J.Y., Valencia, T., Abu-Baker, S., Linares, J., Lee, S.J., Yajima, T., Chen, J., Eroshkin, A., Castilla, E.A., Brill, L.M., et al. (2013). c-Myc phosphorylation by PKCζ represses prostate tumorigenesis. Proc. Natl. Acad. Sci. U S A *110*, 6418–6423.

Kojima, Y., Acar, A., Eaton, E.N., Mellody, K.T., Scheel, C., Ben-Porath, I., Onder, T.T., Wang, Z.C., Richardson, A.L., Weinberg, R.A., and Orimo, A. (2010). Autocrine TGF-beta and stromal cell-derived factor-1 (SDF-1) signaling drives the evolution of tumor-promoting mammary stromal myofibroblasts. Proc. Natl. Acad. Sci. U S A *107*, 20009–20014.

Komatsu, M., Kurokawa, H., Waguri, S., Taguchi, K., Kobayashi, A., Ichimura, Y., Sou, Y.S., Ueno, I., Sakamoto, A., Tong, K.I., et al. (2010). The selective autophagy substrate p62 activates the stress responsive transcription factor Nrf2 through inactivation of Keap1. Nat. Cell Biol. *12*, 213–223.

Levine, B., and Kroemer, G. (2008). Autophagy in the pathogenesis of disease. Cell *132*, 27–42.

Li, L., Shen, C., Nakamura, E., Ando, K., Signoretti, S., Beroukhim, R., Cowley, G.S., Lizotte, P., Liberzon, E., Bair, S., et al. (2013). SQSTM1 is a pathogenic target of 5q copy number gains in kidney cancer. Cancer Cell *24*, 738–750.

Ling, J., Kang, Y., Zhao, R., Xia, Q., Lee, D.F., Chang, Z., Li, J., Peng, B., Fleming, J.B., Wang, H., et al. (2012). KrasG12D-induced IKK2/β/NF-κB activation by IL-1α and p62 feedforward loops is required for development of pancreatic ductal adenocarcinoma. Cancer Cell *21*, 105–120.

Lisanti, M.P., Martinez-Outschoorn, U.E., and Sotgia, F. (2013). Oncogenes induce the cancer-associated fibroblast phenotype: metabolic symbiosis and "fibroblast addiction" are new therapeutic targets for drug discovery. Cell Cycle *12*, 2723–2732.

Locasale, J.W. (2013). Serine, glycine and one-carbon units: cancer metabolism in full circle. Nat. Rev. Cancer *13*, 572–583.

Ma, L., Tao, Y., Duran, A., Llado, V., Galvez, A., Barger, J.F., Castilla, E.A., Chen, J., Yajima, T., Porollo, A., et al. (2013). Control of nutrient stress-induced metabolic reprogramming by PKCζ in tumorigenesis. Cell *152*, 599–611.

Metallo, C.M., and Vander Heiden, M.G. (2013). Understanding metabolic regulation and its influence on cell physiology. Mol. Cell *49*, 388–398.

Moscat, J., and Diaz-Meco, M.T. (2009). p62 at the crossroads of autophagy, apoptosis, and cancer. Cell *137*, 1001–1004.

Moscat, J., and Diaz-Meco, M.T. (2011). Feedback on fat: p62-mTORC1-autophagy connections. Cell *147*, 724–727.

Moscat, J., and Diaz-Meco, M.T. (2012). p62: a versatile multitasker takes on cancer. Trends Biochem. Sci. *37*, 230–236.

Moscat, J., Diaz-Meco, M.T., and Wooten, M.W. (2007). Signal integration and diversification through the p62 scaffold protein. Trends Biochem. Sci. *32*, 95–100.

Nyström, M.L., Thomas, G.J., Stone, M., Mackenzie, I.C., Hart, I.R., and Marshall, J.F. (2005). Development of a quantitative method to analyse tumour cell invasion in organotypic culture. J. Pathol. *205*, 468–475.

Olson, M.V., Lee, J., Zhang, F., Wang, A., and Dong, Z. (2006). Inducible nitric oxide synthase activity is essential for inhibition of prostatic tumor growth by interferon-beta gene therapy. Cancer Gene Ther. *13*, 676–685.

Ostman, A., and Augsten, M. (2009). Cancer-associated fibroblasts and tumor growth—bystanders turning into key players. Curr. Opin. Genet. Dev. *19*, 67–73.

Peña-Llopis, S., Vega-Rubin-de-Celis, S., Schwartz, J.C., Wolff, N.C., Tran, T.A., Zou, L., Xie, X.J., Corey, D.R., and Brugarolas, J. (2011). Regulation of TFEB and V-ATPases by mTORC1. EMBO J. *30*, 3242–3258.

Possemato, R., Marks, K.M., Shaul, Y.D., Pacold, M.E., Kim, D., Birsoy, K., Sethumadhavan, S., Woo, H.K., Jang, H.G., Jha, A.K., et al. (2011). Functional genomics reveal that the serine synthesis pathway is essential in breast cancer. Nature *476*, 346–350.

Ridky, T.W., Chow, J.M., Wong, D.J., and Khavari, P.A. (2010). Invasive three-dimensional organotypic neoplasia from multiple normal human epithelia. Nat. Med. *16*, 1450–1455.

Rolland, P., Madjd, Z., Durrant, L., Ellis, I.O., Layfield, R., and Spendlove, I. (2007). The ubiquitin-binding protein p62 is expressed in breast cancers showing features of aggressive disease. Endocr. Relat. Cancer *14*, 73–80.

Sanchez, P., De Carcer, G., Sandoval, I.V., Moscat, J., and Diaz-Meco, M.T. (1998). Localization of atypical protein kinase C isoforms into lysosome-targeted endosomes through interaction with p62. Mol. Cell. Biol. *18*, 3069–3080.

Santos, A.M., Jung, J., Aziz, N., Kissil, J.L., and Puré, E. (2009). Targeting fibroblast activation protein inhibits tumor stromagenesis and growth in mice. J. Clin. Invest. *119*, 3613–3625.

Schafer, Z.T., and Brugge, J.S. (2007). IL-6 involvement in epithelial cancers. J. Clin. Invest. *117*, 3660–3663.

Schäfer, M., and Werner, S. (2008). Cancer as an overhealing wound: an old hypothesis revisited. Nat. Rev. Mol. Cell Biol. *9*, 628–638.

Schauer, I.G., Ressler, S.J., Tuxhorn, J.A., Dang, T.D., and Rowley, D.R. (2008). Elevated epithelial expression of interleukin-8 correlates with myofibroblast reactive stroma in benign prostatic hyperplasia. Urology *72*, 205–213.

Shen, M.M., and Abate-Shen, C. (2010). Molecular genetics of prostate cancer: new prospects for old challenges. Genes Dev. *24*, 1967–2000.

Thompson, H.G., Harris, J.W., Wold, B.J., Lin, F., and Brody, J.P. (2003). p62 overexpression in breast tumors and regulation by prostate-derived Ets factor in breast cancer cells. Oncogene *22*, 2322–2333.

Trimboli, A.J., Cantemir-Stone, C.Z., Li, F., Wallace, J.A., Merchant, A., Creasap, N., Thompson, J.C., Caserta, E., Wang, H., Chong, J.L., et al. (2009). Pten in stromal fibroblasts suppresses mammary epithelial tumours. Nature *461*, 1084–1091.

Vander Heiden, M.G. (2013). Exploiting tumor metabolism: challenges for clinical translation. J. Clin. Invest. *123*, 3648–3651.

Vander Heiden, M.G., Cantley, L.C., and Thompson, C.B. (2009). Understanding the Warburg effect: the metabolic requirements of cell proliferation. Science *324*, 1029–1033.

Vander Heiden, M.G., Locasale, J.W., Swanson, K.D., Sharfi, H., Heffron, G.J., Amador-Noguez, D., Christofk, H.R., Wagner, G., Rabinowitz, J.D., Asara, J.M., and Cantley, L.C. (2010). Evidence for an alternative glycolytic pathway in rapidly proliferating cells. Science *329*, 1492–1499.

Cancer Cell, Volume *26*

Supplemental Information

Metabolic Reprogramming of Stromal Fibroblasts through p62-mTORC1 Signaling Promotes Inflammation and Tumorigenesis

Tania Valencia, Ji Young Kim, Shadi Abu-Baker, Jorge Moscat-Pardos, Christopher S. Ahn, Miguel Reina-Campos, Angeles Duran, Elias A. Castilla, Christian M. Metallo, Maria T. Diaz-Meco, and Jorge Moscat

Supplemental Data

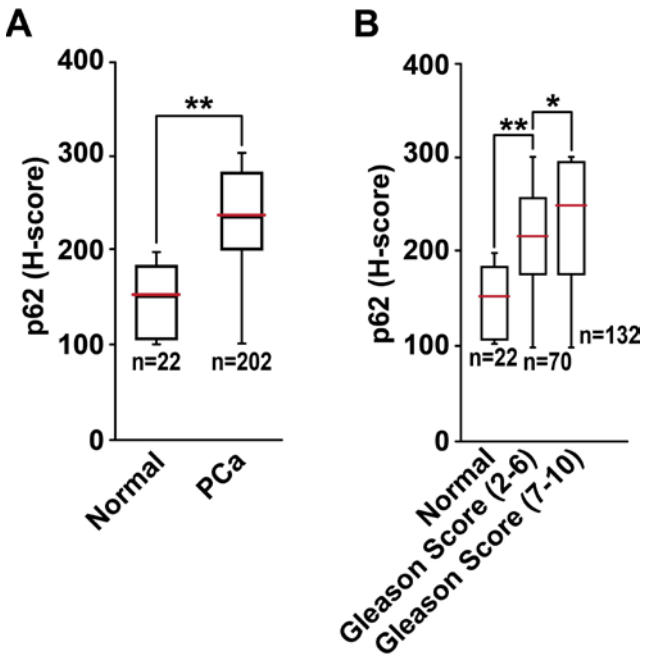

Figure S1, related to Figure 1. p62 is overexpressed in the epithelium of human prostate tumors.

(A) p62 levels are increased in the epithelium of primary PCa tumors as compared to normal samples, and (B) are upregulated upon PCa progression. Analysis of TMA of Figure 1A. The H-score, the staining intensity of p62 in epithelium x the proportion of cells with the observed intensity, was used to grade p62 expression levels in each sample. Students t test (*$p < 0.05$,**$p < 0.01$).

A

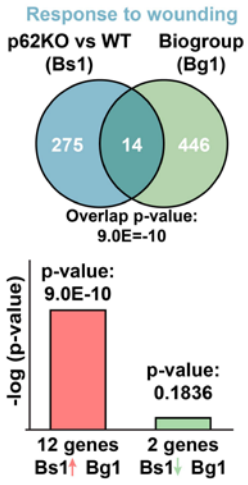

B

Gene sets enriched in phenotype p62 KO- Analysis with C5 database of MSigDB v. 3.1

RANK	MSigDB	Size	ES	NES	NOM p-val	FDR q-val	FWER p-val
1	GENERATION_OF_A_SIGNAL_INVOLVED_IN_CELL_CELL_SIGNALING	26	0.61	1.85	0.001	0.222	0.247
2	G_PROTEIN_SIGNALING_COUPLED_TO_CYCLIC_NUCLEOTIDE_SECOND_MESSENGER	95	0.46	1.82	0	0.166	0.344
3	CYCLIC_NUCLEOTIDE_MEDIATED_SIGNALING	97	0.46	1.78	0	0.181	0.499
4	HUMORAL_IMMUNE_RESPONSE	29	0.56	1.75	0.006	0.182	0.599
5	HORMONE_SECRETION	16	0.64	1.74	0.006	0.172	0.664
6	RESPONSE_TO_WOUNDING	171	0.41	1.73	0	0.15	0.685
7	DETECTION_OF_ABIOTIC_STIMULUS	19	0.61	1.73	0.007	0.137	0.708
8	CELL_CELL_SIGNALING	364	0.38	1.72	0	0.132	0.746
9	RESPONSE_TO_EXTERNAL_STIMULUS	274	0.38	1.71	0	0.125	0.771
10	NEGATIVE_REGULATION_OF_MULTICELLULAR_ORGANISMAL_PROCESS	27	0.55	1.69	0.008	0.14	0.838
11	SECOND_MESSENGER_MEDIATED_SIGNALING	141	0.41	1.69	0	0.137	0.861
12	NEUROLOGICAL_SYSTEM_PROCESS	343	0.37	1.68	0	0.135	0.876
13	INFLAMMATORY_RESPONSE	113	0.41	1.65	0.001	0.172	0.944
14	DETECTION_OF_STIMULUS	41	0.49	1.65	0.006	0.16	0.945
15	ECTODERM_DEVELOPMENT	69	0.44	1.65	0.004	0.15	0.945
16	POTASSIUM_ION_TRANSPORT	56	0.46	1.64	0.004	0.147	0.953
17	REGULATION_OF_MULTICELLULAR_ORGANISMAL_PROCESS	129	0.4	1.64	0.001	0.146	0.959
18	DEFENSE_RESPONSE	209	0.38	1.64	0.001	0.139	0.96
19	G_PROTEIN_SIGNALING_COUPLED_TO_CAMP_NUCLEOTIDE_SECOND_MESSENGER	60	0.45	1.63	0.009	0.136	0.964
20	SYNAPTIC_TRANSMISSION	162	0.38	1.62	0.001	0.141	0.975

C

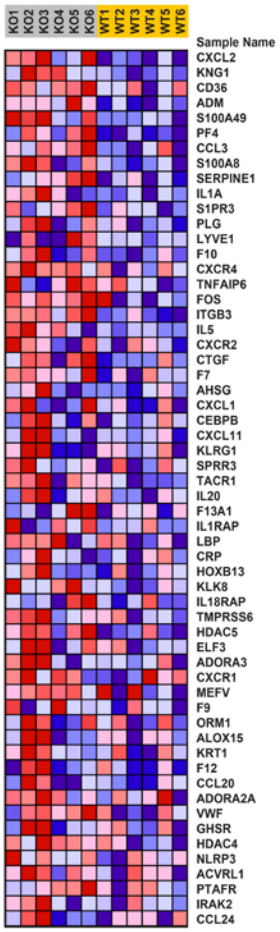

D

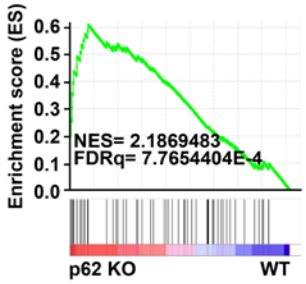

E

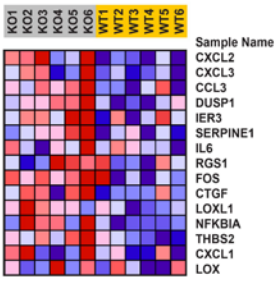

F

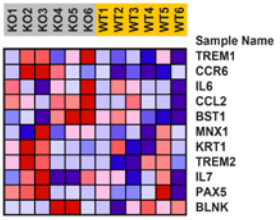

G

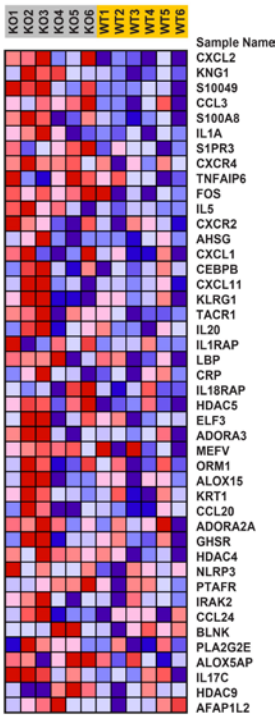

Figure S2, related to Figure 2. p62 deficiency in the stroma promotes a CAF and an inflammatory phenotype.

(A) Genes differentially expressed between orthotopic tumors from WT and p62 KO mice were subjected to NextBio analysis to identify biosets that contain similar genes. Venn diagrams show the number of common and unique genes in both sets. (B and C) Differentially expressed genes in orthotopic tumors from p62 KO mice analyzed by GSEA against C5 biological processes of the MSigDB database. (B) The top-ranked twenty gene sets enriched in p62 KO tumors are shown. (C) Leading edge genes of the “response to wounding” gene set. (D and E) Differentially expressed genes in orthotopic tumors from p62 KO mice analyzed by GSEA against C2 curated gene sets of the MSigDB database. (D) GSEA plot of the selected “stromal stimulation” gene set. (E) Leading edge genes of gene set of D. (F and G) Leading edge genes of selected gene sets enriched in p62 KO tumors from analysis shown in (B).

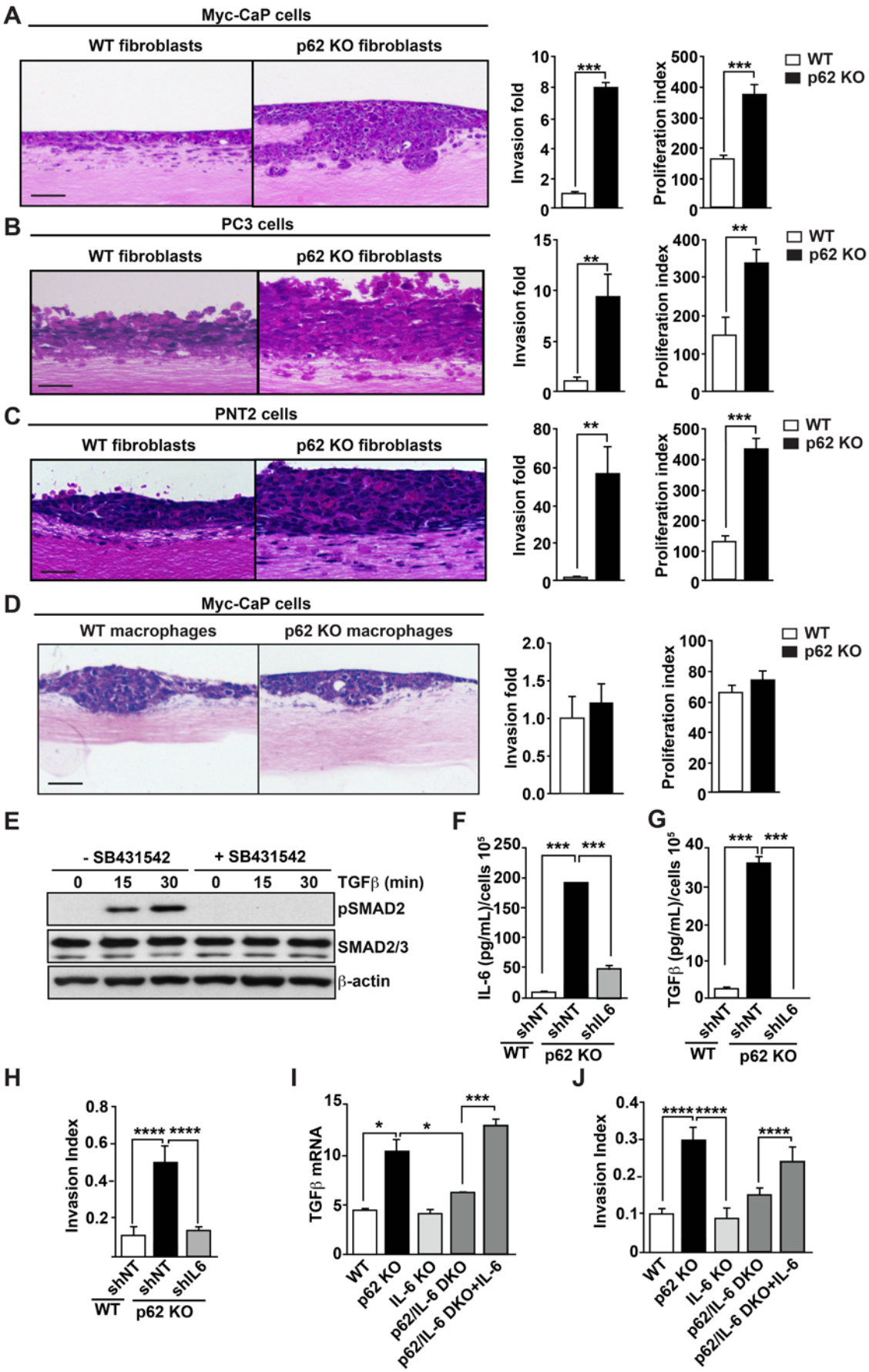
A
Myc-CaP cells
WT fibroblasts
p62 KO fibroblasts
Invasion fold
Proliferation index
WT
p62 KO
B
PC3 cells
C
PNT2 cells
D
Myc-CaP cells
WT macrophages
p62 KO macrophages
E
- SB431542
+ SB431542
0 15 30 0 15 30 TGFβ (min)
pSMAD2
SMAD2/3
β-actin
F
IL-6 (pg/mL)/cells 10^5
G
TGFβ (pg/mL)/cells 10^5
shNT
shIL6
WT
p62 KO
H
Invasion Index
I
TGFβ mRNA
WT
p62 KO
IL-6 KO
p62/IL-6 DKO
p62/IL-6 DKO+IL-6
J
Invasion Index

Figure S3, related to Figure 3. Loss of p62 in the prostate stroma promotes tumorigenesis in the prostate epithelium.

(A-C) H&E-stained organotypic cultures of different type of PCa cells: Myc-CaP (A), PC3 (B) and PNT2 (C) combined with fibroblasts from WT and p62 KO mice. Right panels show quantification of PCa cell invasion and proliferation of the organotypic experiments. (D) H&E-stained organotypic cultures of Myc-CaP cells with macrophages from WT and p62 KO mice. Right panels show quantification of PCa cell invasion and proliferation of the organotypic experiments. (E) The TGFβ inhibitor SB431542 effectively blocks TGFβ signaling as determined by immunoblot with pSMAD2. (F-H) Selective knockdown of IL-6 in p62 KO fibroblasts reverted increased IL-6 (F) and TGFβ (G) production as determined by ELISA, as well as PCa invasion as determined by modified Boyden chamber assay (H). (I) Addition of IL-6 to p62/IL-6 DKO fibroblasts restored TGFβ levels. IL-6 was added for 48 hr and TGFβ mRNA levels were determined by RT-PCR. (J) PCa invasion determined by modified Boyden chamber assay in fibroblasts from the different genotypes. IL-6 was exogenously added to p62/IL-6 DKO fibroblasts. Data are means ± SEM (n = 4). *$p < 0.05$, **$p < 0.01$. ***$p < 0.001$, ****$p < 0.0001$. Scale bars, 100 μm.

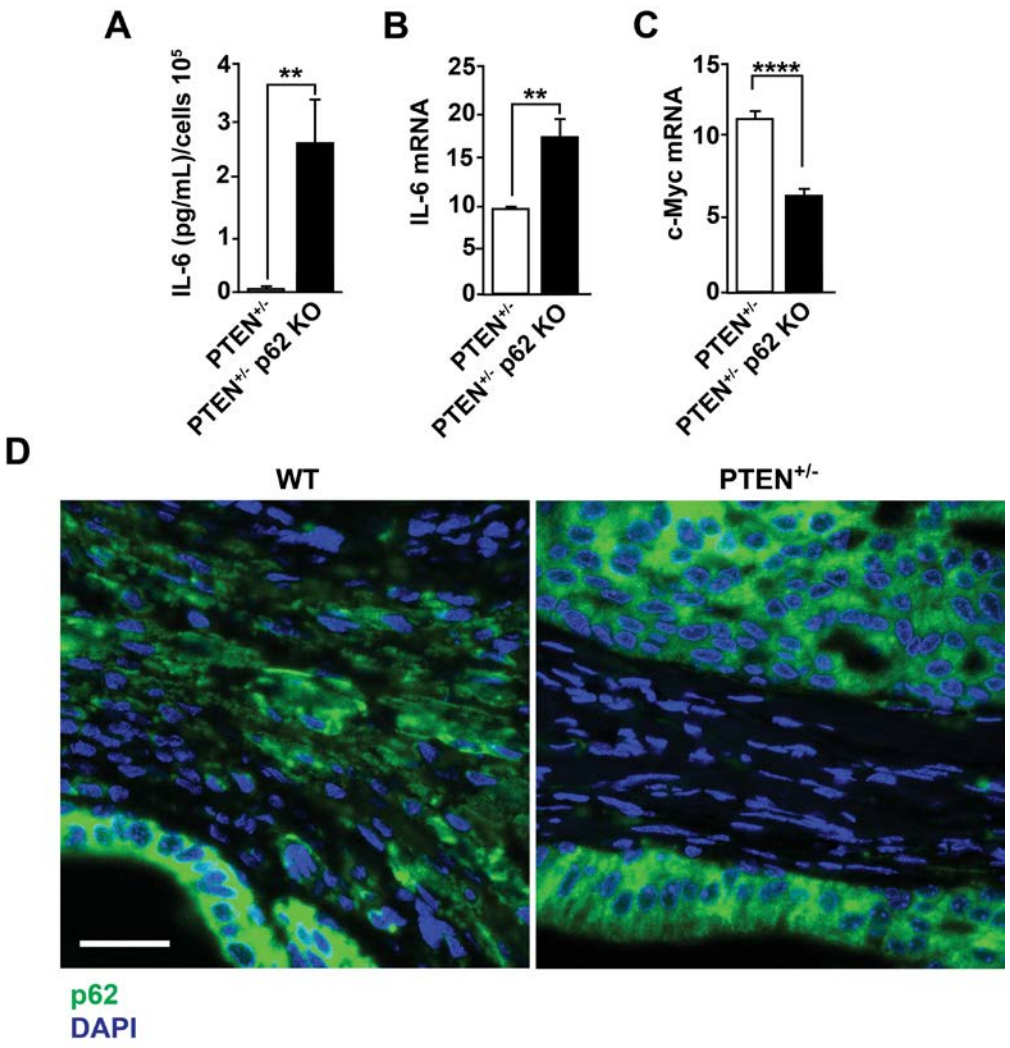

Figure S4, related to Figure 6. p62 role in prostate stroma of PTEN$^{+/-}$ mice.

(A-C) IL-6 ELISA (A) and RT-PCR of IL-6 (B) and c-Myc (C) in prostate stromal cells from PTEN$^{+/-}$ and PTEN$^{+/-}$/p62 KO mice (n = 6). (D) p62 levels are downregulated in the prostate stroma of PTEN$^{+/-}$ mice. Immunostaining of p62 (green) and DAPI (blue) were performed in prostate sections of WT and PTEN$^{+/-}$ mice of 9 months of age (n = 4). **p < 0.01, ****p < 0.0001. Scale bar, 25 μm. Results are presented as means ± SEM.

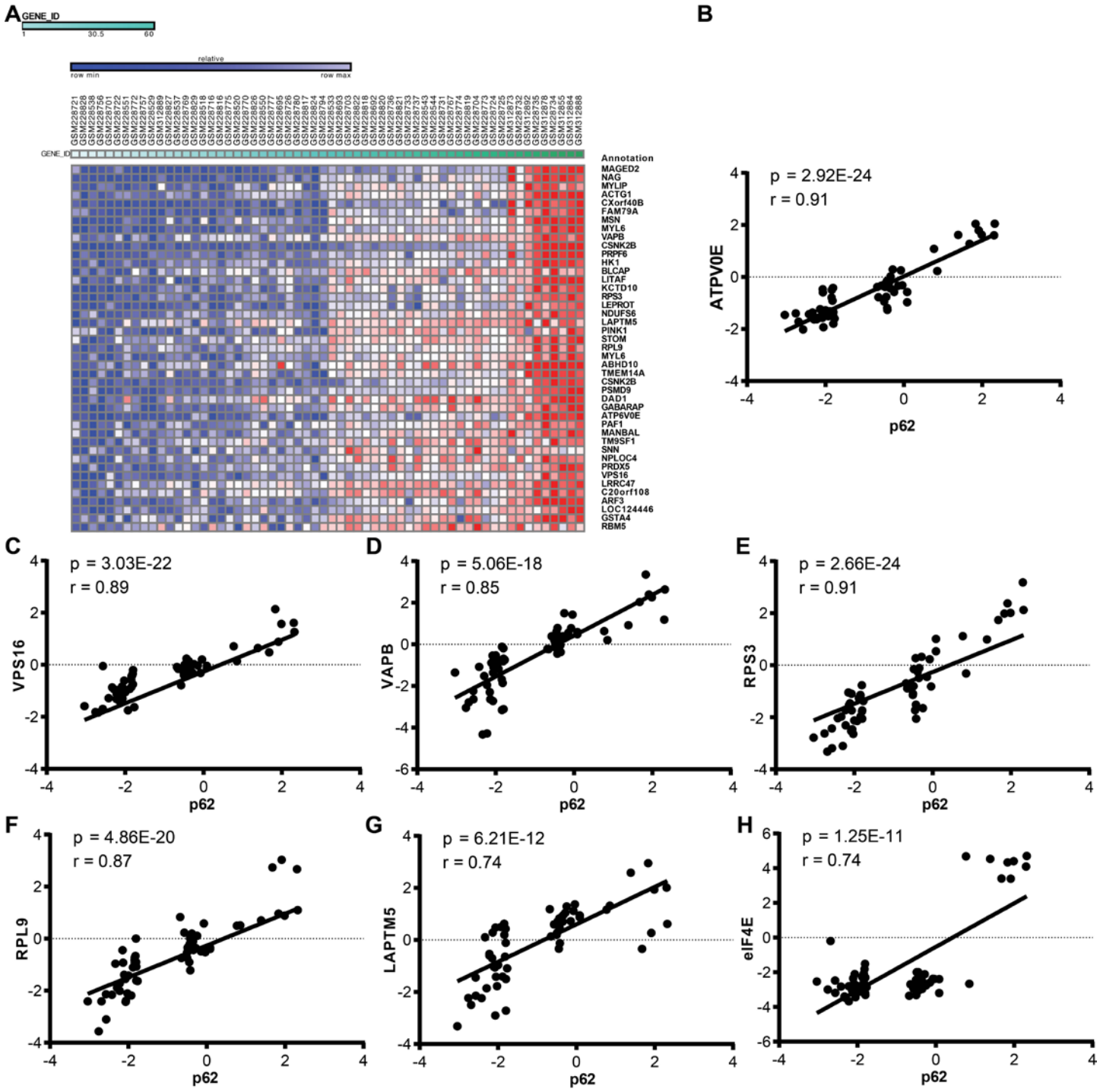
A
GENE_ID
1
30.5
60
relative
row min
row max
GENE_ID
Annotation
MAGED2
NAG
MYLIP
ACTG1
CXorf40B
FAM79A
MSN
MYL6
VAPB
CSNK2B
PRPF6
HK1
BLCAP
LITAF
KCTD10
RPS3
LEPROT
NDUFS6
LAPTM5
PINK1
STOM
RPL9
MYL6
ABHD10
TMEM14A
CSNK2B
PSMD9
DAD1
GABARAP
ATP6V0E
PAF1
MANBAL
TM9SF1
SNN
NPLOC4
PRDX5
VPS16
LRRC47
C20orf108
ARF3
LOC124446
GSTA4
RBM5
B
p = 2.92E-24
r = 0.91
ATPV0E
p62
C
p = 3.03E-22
r = 0.89
VPS16
p62
D
p = 5.06E-18
r = 0.85
VAPB
p62
E
p = 2.66E-24
r = 0.91
RPS3
p62
F
p = 4.86E-20
r = 0.87
RPL9
p62
G
p = 6.21E-12
r = 0.74
LAPTM5
p62
H
p = 1.25E-11
r = 0.74
eIF4E
p62

Figure S5, Related to Figure 7. p62 signature in human stroma.

(A) Heat map of the top 25 genes differentially expressed (FDR > 0.0002 and fold > 1.5) in the top 25% versus the bottom 25% of human stroma samples ranked by p62 expression levels. Expression data were extracted from the GSE9014 dataset. Blue and red in the heatmap indicate genes that are underexpressed or overexpressed, respectively. (B-H) A positive significant correlation of gene expression between p62 and ATPV0E (B), VPS16 (C), VAPB (D), RSP3 (E), RPL9 (F), LAPTM5 (G), and eIF4E (H) is shown for human stromal samples from the GSE9014 dataset.

Supplemental Experimental Procedures

Materials

Reagents were obtained from the following sources: Antibodies to KEAP1, actin, and HRP-labeled anti-mouse were from Santa Cruz Biotechnology. Antibodies to phospho-T389 S6K1, phospho-T37/46 4EBP1, phospho-Smad2-S465/467, HRP-labeled anti-rabbit secondary antibody and rapamycin were from Cell Signaling Technology. Antibody to Ki-67 was from ThermoScientific. Antibody to BrdU was from Millipore. Antibody to c-Myc [Y69] was from Abcam. Collagen, Matrigel, invasion chambers, NuSerum and antibody to human p62 were from BD biosciences; Antibody to murine p62 was from ThermoScientific. TGFβ and murine IL-6 was obtained from PeproTech. FLAG antibody, Butylated hydroxyanisole (BHA), Gluthatione Ethyl Ester (GEE), torin1, testosterone, methanol, chloroform, norvaline, 5-bromo-2'-deoxyuridine, and the glutathione assay kit were from Sigma Aldrich. TGFβ inhibitor, SB431542 was from StemRD. DMEM and fetal bovine serum were from Hyclone; X-tremeGENE and Dnase were from Roche. OneComp ebeads, antibodies CD31-FITC (clone 390), CD45-FITC (clone 30-F11), Ter119-FITC (clone TER-119), Sca-1-APC (clone D7), CD49f-PE (clone eBioGoH3), and TGF beta ELISA Ready-SET-GO were from eBioscience. αSMA was from DAKO. Trypsin, Insulin and collagenase were from Gibco. Crystal violet and 10% formalin were from Fisher Scientific. RNeasy RNA extraction kit was from Qiagen. High-Capacity cDNA reverse transcription kit was from Applied Biosystems. iTaq Universal SYBR green supermix was from Biorad. NADP/NADPH quantification colorimetric kit was from Biovision. CM-H_2DCFDA was from Molecular Probes. Alexa Fluor 488 tyramide signal amplification kit was from Life Technologies.

Cell Culture

HEK293T and PC-3 were from American Type Culture Collection (ATCC). PNT2 was obtained from Sigma. The Myc-CaP cell line was a generous gift from Dr. Charles Sawyers.

WT and p62 KO stromal prostate fibroblasts were isolated from mouse prostate, as described previously (Tuxhorn et al., 2002). Murine TRAMP-C2Re3 cells were previously described (Olson et al., 2006). Stromal prostate fibroblast cells were cultured in Dulbecco's modified Eagle's medium (DMEM) supplemented with 5% (vol/vol) fetal bovine serum (FBS), 5% (vol/vol) NuSerum IV, 1% glutamine, 1% penicillin-streptomycin, 0.01 μM testosterone, and 25 μg ml^{-1} of insulin, in an atmosphere of 95% air and 5% CO_2 at 37°C. Cells were stimulated with inhibitors (rapamycin, 100 nM; torin1, 100 nM; SB431542, 10 μM) or antioxidants (BHA [100 □M] and GEE [0, 2.5, 5.0, 10 mM]) for 12 h.

Mammalian Lentiviral shRNAs and Retroviral Transduction

pWZL-Hygro (Addgene plasmid 18750, donated by Scott, L), pWZL-Blast-Myc (Addgene, plasmid 10674) (Boehm et al., 2005), FLAG pLJM1 RagB 99L (Addgene, plasmid 19315) (Sancak et al., 2008), TRC lentiviral shRNA targeting murine c-Myc (TRCN0000234923) was obtained from Sigma Aldrich. TRC lentiviral shRNA targeting murine IL-6 (TRCN0000067548) was obtained from OpenBioSystems, Thermo Scientific. Actively growing HEK293T cells were co-transfected with shRNA-encoding plasmids, psPAX2 (Addgene, plasmid 12260) and pMD2.G (Addgene, plasmid 12259) packaging plasmids using X-tremeGENE transfection reagent. For retroviruses, pWZL-encoding plasmids were transfected into actively growing Phoenix cells with X-tremeGENE transfection reagent to produce viral particles, which were used to infect cells. Virus-containing supernatants were collected 48 and 72 hr post-transfection and filtered to remove cells. Target cells were infected in the presence of 8 μg ml^{-1} polybrene. Cells were selected with puromycin, hygromycin, or blasticidin after infection.

Gene-expression analyses

RNA was isolated using RNeasy mini kit from Qiagen (Valencia, USA). Total RNA (1 µg) was reverse-transcribed using the High-Capacity cDNA Reverse Transcription Kit (Applied Biosystems). Quantitative real-time PCR was performed using iTaq Universal SYBR green supermix (Biorad) on a Biorad CFX96 detection system. PCR primers were designed using the online primer tool Primer3 and purchased from Integrated DNA Technologies. 18S was used as the housekeeping gene for normalization, with a melting curve performed after each reaction.

Histological analysis

Excised prostates were fixed in 10% formalin, dehydrated, and embedded in paraffin. Samples were sectioned at 5 µm and subjected to staining with hematoxylin and eosin. For immunohistochemistry, samples were dewaxed and stained with anti-αSMA (clone 1A4, 1:400 dilution), with a ready to use anti-Ki-67 (1:10 dilution), or with anti-BrdU (clone PRB-1, 1:200 dilution). Secondary biotinylated antibody and ABC complex (Vectastain Elite, Vector Labs) were used for detection following manufacturer's instructions. Human prostate tissue microarrays (TMA) were obtained from US Biomax. This study had Institutional Review Board exempt status due to de-identification of the human samples. TMA were stained with anti-p62. TMA slides were scanned and imaged using the Scanscope XT system (Aperio) and Aperio ImageScope software, respectively. The scoring of staining intensity was done by a pathologist (E.C) in a blinded fashion. For immunofluorescence, sections were deparafinized as described above and incubated with anti-p62 antibody (1:100) overnight at 4°C. Alexa Fluor 488 tyramide signal amplification kit for p62 antibody was used. Stained sections were examined under an inverted laser scan microscope (LSM 710 NLO, Zeiss, Germany).

FACs-sorted murine stromal isolation

Prostates from 12-week-old mice were harvested and dissected. Prostate cell isolation has been described previously (Lukacs et al., 2010). Cells were stained with fluorescently labeled lineage markers (CD31-FITC, CD45-FITC, and Ter119-FITC), CD49f-PE, and Sca-1-APC. Unstained prostate cells were used as the control to set the background fluorescence. Single-color stained OneComp ebeads (eBioscience) were used for FACS Aria cell sorter equipment compensation. FMO compensations were also performed. Stromal cells were sorted at 4°C into FACS Collection media using the FACS Aria cell sorter and FACS Diva software (BD Biosciences). Stromal cell fractions were sorted based on the Lin^-, $Sca\text{-}1^+$, $CD49f^-$ profile.

Determination of ROS Levels

Cells were washed once with warm PBS and were incubated with 10 μM 5-(and-6)-chloromethyl-2',7'-dichlorodihydrofluorescein diacetate, acetyl ester (CM-H_2DCFDA, Molecular Probes) in warm PBS. After 30 min at 37°C, cells were washed, trypsinized, and re-suspended in PBS. Detection of ROS levels was carried out through flow cytometric analyses using a FACS Canto flow cytometer (Becton-Dickinson) with FlowJo software (BD Biosciences).

Measurement of NADPH/NADP ratio and GSH intracellular levels

Fibroblast cells were washed with cold PBS and extracted with NADP/NADPH extraction buffer. Quantification was carried out using the NADP/NADPH quantification colorimetric kit (Cat. No. K347-100, BioVision) according to the manufacturer's protocol. GSH was measured using the Glutathione Assay Kit (Cat No. CS0260, Sigma Aldrich). The plate reader was set to 412 nm with kinetic reads at 1 min intervals for 5 min. At least three independent measurements were carried out.

ELISAS

Culture supernatants were harvested, clarified by centrifugation, and frozen for the subsequent determination of IL-6 concentration by enzyme-linked immunosorbent assay (ELISA) according to the manufacturer's instructions (BD Bioscience). TGFβ□levels in culture supernatants were quantified using the Human/Mouse TGF beta 1 ELISA Ready-SET-Go! (eBioscience).

Invasion Assay

PCa cells (5 x 10^4) were plated onto 8 µm-pore Matrigel Invasion chambers (BD Biosciences) in 24-well plates. Conditioned media from WT, p62 KO, IL-6 KO, p62/IL-6 DKO, p62/IL-6 DKO + IL-6, WT shNT, p62 KO shNT, p62 KO shIL-6 fibroblasts were added to the lower chamber as a chemoattractant. Cells were allowed to invade for 22 hr at 37°C. Non-invading cells in the upper surface were removed and those on the lower surface fixed in methanol and stained with crystal violet. Cells in at least five randomly selected fields from each of three experiments were counted.

Co-culture invasion assays

Invasion assays were performed as described above with a few modifications. WT shNT or WT shMyc fibroblast (7.5 x 10^4) were seeded in TC-treated 24-well plates and allowed to attach for 6 hr before PCa cells were seeded on top of the invasion chamber. The chamber was then placed in the pre-seeded 24-well plate. Invasion was quantified after 22 hr.

Organotypic cultures

3D air liquid organotypic culture cultures have been used extensively in skin (Gaggioli et al., 2007), esophageal (Okawa et al., 2007), pancreas (Coleman et al., 2014), colon (Henriksson et al., 2011), breast (Chioni and Grose, 2012) and more recently in prostate cancer (Kim et al.,

2013), to determine the mechanisms of tumor invasion and the role of the stromal compartment (Chioni and Grose, 2008). To study the interaction between the prostate cancer cells and surrounding stroma to impact cancer cell proliferation and invasion, a 3D air liquid organotypic culture was set up as previously described (Kim et al., 2013) (Coleman et al., 2014). Briefly, gels were composed of one ml of a mixture of 1.75 volumes of Matrigel, 5.25 volumes of collagen type I, 1 volume of 1x DMEM, 1 volume of 10x DMEM, and 1 volume of filtered FBS. The mixture was plated onto 24-well plates coated with diluted collagen type I. Gels were allowed to equilibrate with 1 ml of 1x DMEM overnight at 37°C. 5 x 10^5 cells PCa cells and prostate stromal cells (50:50) were then seeded on top of the matrix as shown in the scheme below. For organotypic cultures with macrophages, whole bone marrow cells were obtained from WT and p62 KO mice and differentiated as previously described (Lee et al., 2010). Differentiated macrophages were embedded into the organotypic gels and PCa cells were seeded on top of the gel. Gel rafts were placed onto collagen-coated nylon sheets and lifted using a sterile supporting steel mesh to set up a raised air-liquid culture. Normal medium was changed in alternate days and organotypic cultures were allowed to grow for 14 days. Afterwards, organotypic gels were harvested, fixed in 10% neutroal buffered formalin, bisected and embedded in paraffin. H&E stained sections were analyzed with a Zeiss light microscope supplemented with Axiovision40 software. Quantification of the invasion assays was performed as described previously (Nystrom et al., 2005) using ImageProPlus software.

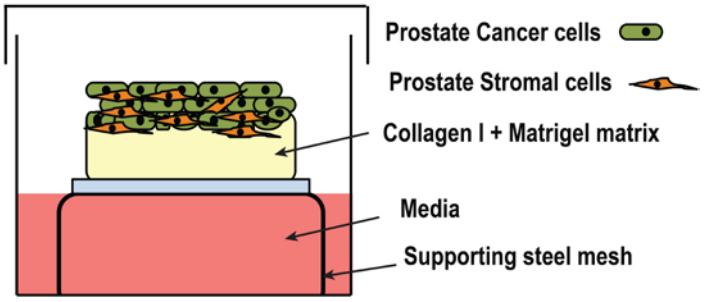

Schematic representation of air-liquid organotypic cultures

In vivo orthotopic tumor assay

Murine TRAMP-C2Re3 prostate carcinoma cells (5×10^4) were injected orthotopically into the prostates of WT, p62 KO, and p62/IL-6 DKO mice and harvested after 60 days, as previously described (Olson et al., 2006).

Xenograft experiments

Cell mixtures (1×10^6 cells) of equal ratios of PCa cells with fibroblasts in a 100 µl of BD Matrigel (BD Biosciences) were injected into the flanks of WT mice. Tumors were allowed to grow for 6 weeks. Tumor volume was measured every week.

Metabolic Extraction

For labeling experiments, 2×10^5 cells were seeded in 6-well plates. After 16 hr of incubation, cells were washed with PBS and incubated with DMEM, 10% dialyzed serum, and either 4 mM [U-$^{13}C_5$]glutamine and 25 mM unlabeled glucose or [1,2$^{13}C_2$]glucose and unlabeled glutamine. Spent medium from labeled cells was collected and analyzed for glucose, glutamine consumption, and lactate production using the YSI2950 analyzer. Cells were rinsed in ice-cold saline solution, and then ice-cold 100% HPLC-grade methanol was added to the cells. An equal volume of water containing norvaline as standard was added to the plate. Cells were scraped and mixed with ice-cold chloroform. Samples were vortexed for 10 min at room temperature and centrifuged at 3000 g for 10 min. Polar metabolites were separated and evaporated in a refrigerated vacuum centrifuge.

Derivatization, gas chromatography/mass spectrometry (GC/MS) analysis, and flux calculations

Polar metabolites were derivatized to form methoxime-tBDMS derivatives by first dissolving the evaporated samples in 20 µl of 2% (w/v) methoxylamine hydrochloride (MP Biomedicals, OH) in pyridine and incubating at 37°C for 60 min. Samples were then silylated by addition of 30 µl of N-tertbutyldimethylsily-N-methyltrifluoroacetamide (MTBSTFA) with 1% tert-butyldimethylchlorosilane (TBDMCS) (Regis Technologies, IL) and incubated at 37°C for 45 min. Samples were centrifuged at 14,000 rpm for 5 min and clarified supernatant was transferred to GC sample vials for analysis. Derivatized samples were analyzed by GC-MS using a DB-35MS (Agilent J&W Scientific) installed in an Agilent 7890A GC interfaced with an Agilent 5975C MS operating in electron impact mode scanning over the range 100-650 m/z. The GC method and metabolite peaks used for integration have been previously described (Grassian et al., 2011) (Metallo et al., 2012). Uptake and secretion fluxes of glucose, glutamine, and lactate were then calculated using an exponential growth model. PPP flux was determined by multiplying lactate secretion flux by the ratio of M1 to M2 lactate labeled from [1,2-$^{13}C_2$]glucose as described above.

Array and Gene Set Enrichment Analysis

Microarray studies were performed in the Genomics and Microarray Laboratory at the Department of Environmental Health, University of Cincinnati Medical Center. Briefly, total RNA was extracted from six independent orthotopic tumors from WT and p62 KO mice and hybridized on Affymetrix mouse ST 1.0 microarrays. Scanning of the images and the first pass processing of probe-level fluorescence intensities was performed using the Microarray Suite 5.0 software (MAS 5.0; Affymterix, Santa Clara, CA). The data was normalized, and the calculation of the gene-specific summary measures was performed by the robust multi-array average

(RMA) procedure (Irizarry et al., 2003) based on the Entrez gene-centric probe set definitions provided by the University of Michigan "brainarray" group (Dai et al., 2005). Statistical significance of genes differentially expressed between WT and p62 KO orthotopic tumors were assessed using Empirical Bayes linear model (Sartor et al., 2006). Gene set enrichment analysis was performed using GSEA v2.0.14 software (http://www.broadinstitute.org/gsea/index.jsp) with 5000 gene set permutations using the metric Signal-to-Noise ratio (S2N) and the collection C5.bp.v3.1.symbols or C2.all.v4.0.symbols (Subramanian et al., 2005Subramanian et al., 2005). Probe sets were collapsed using MoGene_1_0_st.chip. Meta-analyses to identify overlapping and associated genes with publically available data set were performed using the NextBio™ (NextBio, Cupertino, CA) on-line search engine (www.nextbio.com). Differentially expressed genes were further analyzed with the Ingenuity Pathways Analysis program (http://www.ingenuity.com/index.html).

Supplemental References

Boehm, J.S., Hession, M.T., Bulmer, S.E., and Hahn, W.C. (2005). Transformation of human and murine fibroblasts without viral oncoproteins. Mol Cell Biol 25, 6464-6474.

Chioni, A.M., and Grose, R. (2008). Organotypic modelling as a means of investigating epithelial-stromal interactions during tumourigenesis. Fibrogenesis & tissue repair 1, 8.

Chioni, A.M., and Grose, R. (2012). FGFR1 cleavage and nuclear translocation regulates breast cancer cell behavior. The Journal of cell biology 197, 801-817.

Coleman, S.J., Chioni, A.M., Ghallab, M., Anderson, R.K., Lemoine, N.R., Kocher, H.M., and Grose, R.P. (2014). Nuclear translocation of FGFR1 and FGF2 in pancreatic stellate cells facilitates pancreatic cancer cell invasion. EMBO Mol Med 6, 467-481.

Dai, M., Wang, P., Boyd, A.D., Kostov, G., Athey, B., Jones, E.G., Bunney, W.E., Myers, R.M., Speed, T.P., Akil, H., et al. (2005). Evolving gene/transcript definitions significantly alter the interpretation of GeneChip data. Nucleic acids research 33, e175.

Grassian, A.R., Metallo, C.M., Coloff, J.L., Stephanopoulos, G., and Brugge, J.S. (2011). Erk regulation of pyruvate dehydrogenase flux through PDK4 modulates cell proliferation. Genes & development 25, 1716-1733.

Henriksson, M.L., Edin, S., Dahlin, A.M., Oldenborg, P.A., Oberg, A., Van Guelpen, B., Rutegard, J., Stenling, R., and Palmqvist, R. (2011). Colorectal cancer cells activate adjacent fibroblasts resulting in FGF1/FGFR3 signaling and increased invasion. The American journal of pathology 178, 1387-1394.

Irizarry, R.A., Hobbs, B., Collin, F., Beazer-Barclay, Y.D., Antonellis, K.J., Scherf, U., and Speed, T.P. (2003). Exploration, normalization, and summaries of high density oligonucleotide array probe level data. Biostatistics 4, 249-264.

Lee, S.J., Kim, J.Y., Nogueiras, R., Linares, J.F., Perez-Tilve, D., Jung, D.Y., Ko, H.J., Hofmann, S.M., Drew, A., Leitges, M., et al. (2010). PKCzeta-regulated inflammation in the nonhematopoietic compartment is critical for obesity-induced glucose intolerance. Cell Metab 12, 65-77.

Lukacs, R.U., Goldstein, A.S., Lawson, D.A., Cheng, D., and Witte, O.N. (2010). Isolation, cultivation and characterization of adult murine prostate stem cells. Nat Protoc 5, 702-713.

Metallo, C.M., Gameiro, P.A., Bell, E.L., Mattaini, K.R., Yang, J., Hiller, K., Jewell, C.M., Johnson, Z.R., Irvine, D.J., Guarente, L., et al. (2012). Reductive glutamine metabolism by IDH1 mediates lipogenesis under hypoxia. Nature 481, 380-384.

Okawa, T., Michaylira, C.Z., Kalabis, J., Stairs, D.B., Nakagawa, H., Andl, C.D., Johnstone, C.N., Klein-Szanto, A.J., El-Deiry, W.S., Cukierman, E., et al. (2007). The functional interplay between EGFR overexpression, hTERT activation, and p53 mutation in esophageal epithelial

cells with activation of stromal fibroblasts induces tumor development, invasion, and differentiation. Genes & development 21, 2788-2803.

Sancak, Y., Peterson, T.R., Shaul, Y.D., Lindquist, R.A., Thoreen, C.C., Bar-Peled, L., and Sabatini, D.M. (2008). The Rag GTPases bind raptor and mediate amino acid signaling to mTORC1. Science 320, 1496-1501.

Sartor, M.A., Tomlinson, C.R., Wesselkamper, S.C., Sivaganesan, S., Leikauf, G.D., and Medvedovic, M. (2006). Intensity-based hierarchical Bayes method improves testing for differentially expressed genes in microarray experiments. BMC bioinformatics 7, 538.

Subramanian, A., Tamayo, P., Mootha, V.K., Mukherjee, S., Ebert, B.L., Gillette, M.A., Paulovich, A., Pomeroy, S.L., Golub, T.R., Lander, E.S., et al. (2005). Gene set enrichment analysis: a knowledge-based approach for interpreting genome-wide expression profiles. Proc Natl Acad Sci U S A 102, 15545-15550.

Tuxhorn, J.A., McAlhany, S.J., Dang, T.D., Ayala, G.E., and Rowley, D.R. (2002). Stromal cells promote angiogenesis and growth of human prostate tumors in a differential reactive stroma (DRS) xenograft model. Cancer Res 62, 3298-3307.